

# Onset of carbonate biomineralization drove global reorganization of sedimentation and subsidence patterns

Kristin D Bergmann<sup>1</sup>, Julia Wilcots<sup>1</sup>, Tamara Pico<sup>2</sup>, Nicholas Boekelheide<sup>1</sup>, Noah T Anderson<sup>1</sup>, Marjorie D Cantine<sup>1</sup>, Samuel L Goldberg<sup>1</sup>, Brenhin Keller<sup>3</sup>, Adam B Jost<sup>1</sup>, and Athena Eyster<sup>1</sup>

<sup>1</sup>Massachusetts Institute of Technology

<sup>2</sup>University of California, Santa Cruz

<sup>3</sup>Dartmouth College

November 22, 2022

## Abstract

Carbonate rocks on continental crust are one of Earth's largest reservoirs of CO<sub>2</sub> and yet the controls on their volume through time are poorly understood. Here we quantify temporal changes in preserved continental carbonate rocks over the last billion years in both global and North America-specific datasets within paleogeographic context. We find the preserved area of continental carbonate rocks increases by ~175% across the Neoproterozoic-Phanerozoic boundary ca. 539 million years ago, coincident with the rise of macroscopic, multicellular life and the evolutionary innovation of carbonate biomineralization in shallow water reefs. We demonstrate that crustal loading from carbonate sediments on one tropical paleo-continent (North America) contributes to an increase in continent-scale accommodation in the early Phanerozoic, expanding shallow marine environments. We predict this feedback between enhanced carbonate accumulation and subsidence was an important component of the termination of the Great Unconformity. These results are combined into a new conceptual model that links the changes in preserved carbonate rock volumes to the evolutionary innovation of carbonate biomineralization in a range of complex organisms. Our model implies evolutionary controls on the carbonate rock reservoir enhanced CO<sub>2</sub> sequestration at the beginning of the Phanerozoic, with consequences for Earth's carbon cycle, climate and habitability.

1 Title:  
2 Onset of carbonate biomineralization drove global  
3 reorganization of sedimentation and subsidence  
4 patterns

5 Kristin D. Bergmann<sup>1\*</sup>, Julia Wilcots<sup>1</sup>, Tamara Pico<sup>2</sup>, Nicholas Boekelheide<sup>1</sup>,  
Noah T. Anderson<sup>1</sup>, Marjorie D. Cantine<sup>1,3</sup>, Samuel L. Goldberg<sup>1,4</sup>,  
Brenhin Keller<sup>5</sup>, Adam B. Jost<sup>1</sup>, Athena Eyster<sup>1,6</sup>

<sup>1</sup>Department of Earth, Atmospheric and Planetary Sciences, Massachusetts Institute of Technology,  
Cambridge, MA 02139

<sup>2</sup>Department of Earth and Planetary Sciences, University of California, Santa Cruz  
Santa Cruz, CA 95064

<sup>3</sup>now at Department of Geosciences, Goethe-Universität  
Frankfort, Germany

<sup>4</sup>now at Rosenstiel School of Marine and Atmospheric Science, University of Miami  
Miami, FL 33149

<sup>5</sup>Department of Earth Sciences, Dartmouth College  
Hanover, NH 03755

<sup>6</sup>now at Department of Geoscience, University of Wisconsin, Madison  
Madison, WI 53706

\*To whom correspondence should be addressed; E-mail: [kdberg@mit.edu](mailto:kdberg@mit.edu).

6 **Carbonate rocks on continental crust are one of Earth's largest reservoirs of**  
7 **CO<sub>2</sub> and yet the controls on their volume through time are poorly understood.**  
8 **Here we quantify temporal changes in preserved continental carbonate rocks**  
9 **over the last billion years in both global and North America-specific datasets**

10 within paleogeographic context. We find the preserved area of continental  
11 carbonate rocks increases by  $\sim 175\%$  across the Neoproterozoic–Phanerozoic  
12 boundary ca. 539 million years ago, coincident with the rise of macroscopic,  
13 multicellular life and the evolutionary innovation of carbonate biomineraliza-  
14 tion in shallow water reefs. We demonstrate that crustal loading from carbon-  
15 ate sediments on one tropical paleo-continent (North America) contributes to  
16 an increase in continent-scale accommodation in the early Phanerozoic, ex-  
17 panding shallow marine environments. We predict this feedback between en-  
18 hanced carbonate accumulation and subsidence was an important component  
19 of the termination of the Great Unconformity. These results are combined into  
20 a new conceptual model that links the changes in preserved carbonate rock  
21 volumes to the evolutionary innovation of carbonate biomineralization in a  
22 range of complex organisms. Our model implies evolutionary controls on the  
23 carbonate rock reservoir enhanced  $\text{CO}_2$  sequestration at the beginning of the  
24 Phanerozoic, with consequences for Earth’s carbon cycle, climate and habit-  
25 ability.

26 One sentence summary: Biomineralization innovations drove increases in the volume of  
27 carbonate deposition, global changes in sedimentation patterns, and loading of the crust.

28 **Main Text:** The Cambrian Explosion and the Great Ordovician Biodiversification Event in  
29 the early Phanerozoic (538.8– $\sim 440$  Ma), together are the earliest diversification of animals,  
30 including those capable of biomineralization. These evolutionary milestones coincide with  
31 striking, enigmatic features of the rock record including: 1) a widespread shift to carbonate  
32 deposition in shallow continental seas reaching far into continental interiors following flood-  
33 ing in the early Phanerozoic. This continental flooding terminates what is known as the Great

34 Unconformity, a time gap between older igneous and sedimentary rocks and Phanerozoic-aged  
35 sedimentary rocks (538.8–0 Ma) (1, 2), 2) a transition from large magnitude carbon isotope  
36 perturbations in carbonate and organic carbon in the Neoproterozoic (1000–538.8 Ma) to more  
37 muted  $\delta^{13}\text{C}$  excursions in most of the Phanerozoic (Fig. 1A) (3), 3) a secular increase in  $\delta^{18}\text{O}$   
38 values of well-preserved fossils, consistent with long-term global cooling in the early Phanero-  
39 zoic (Fig. 1B) (4–8), and 4) a shift from rare but extreme Snowball Earth glaciations that  
40 extended to low-latitudes in the Proterozoic (1000–538.8 Ma) to high latitude glaciations in the  
41 Phanerozoic (9–12). The co-occurrence of these four enigmatic features of the rock record with  
42 the diversification of macroscopic animal life suggest there may be unidentified connections  
43 between relative sea-level, carbon cycle dynamics, climate, atmospheric oxygen and Earth's  
44 habitability (9, 10, 13–15).

45 Today, carbon and  $\text{CO}_2$  are unequally divided between Earth's ocean, atmosphere, terrestrial,  
46 and crustal reservoirs, with approximately 80% of near-surface carbon or  $6 \times 10^7$  GtC stored  
47 in carbonate rocks on continental crust (16)—changes in the size of this reservoir could have  
48 large effects on the global carbon cycle. Projecting observations from the modern carbon cy-  
49 cle backwards in time is a common approach when interpreting the ancient Earth system, yet  
50 how far back in time is it reasonable to project modern carbon cycle reservoir sizes and fluxes?  
51 Punctuated, sweeping changes to both carbon cycling and storage have been triggered by evo-  
52 lutionary innovations in the biosphere. Early land plant evolution ( $\sim 400$ –350 Ma), enhanced  
53 weathering and organic carbon burial on continental crust (17). The evolutionary diversification  
54 of millimeter-scale planktonic organisms that precipitate  $\text{CaCO}_3$  skeletons in surface waters far  
55 from coasts ( $\sim 220$ –145 Ma) added a new locus of carbonate deposition in deep water environ-  
56 ments (15, 18–20) (Fig. 1H). In modern oceans, these organisms efficiently sequestering  $\text{CO}_2$   
57 and effectively contributing  $\text{CO}_2$  to both the mantle and the atmosphere after subduction of

58 oceanic crust (15, 20–22).

59 The advent of carbonate biomineralization in early complex, macroscopic animals and algae  
60 in the early Phanerozoic represents another possible punctuated, large-scale change to a key  
61 reservoir in Earth’s carbon cycle (Fig. 1G). This evolutionary event drove a shift from abiotic  
62 and microbially-mediated carbonates, like stromatolites, in Proterozoic (2500–538.8 Ma) reefs  
63 to abundant, thick-shelled, seafloor-dwelling carbonate biomineralizing organisms in Phanero-  
64 zoic reefs. Despite the fact that this transformation of nearshore reefs occurs within one of  
65 Earth’s largest carbon reservoirs, carbonate rocks on continental crust, its relative impact as a  
66 driver of large-scale carbon-cycle change is less well understood than the rise of land plants  
67 or planktonic calcifying organisms. This is, in large part, because skeletons from carbonate  
68 biomineralizers do not clearly represent a new carbon sink as carbonate producing shallow-  
69 water ecosystems existed throughout the last 3.4 billion years of Earth’s history.

70 Here we explore whether the emergence of biomineralization was a critical driver of early  
71 Phanerozoic flooding and changes in the early Phanerozoic carbon cycle and climate. Address-  
72 ing this question requires a quantitative assessment of the types of sediment being deposited  
73 globally through time and their impacts on subsidence and the creation of accommodation, or  
74 the space to deposit new sediment. Here we quantify temporal changes in preserved continen-  
75 tal carbonate sediments with global, lithology-specific, paleogeographic context over the last  
76 billion years. To better constrain the continental carbonate rock reservoir preserved on either  
77 side of the Neoproterozoic–Phanerozoic boundary, our approach expands efforts that explored  
78 preserved continental sedimentary rock patterns that were temporally limited to the Phanero-  
79 zoic (23–28), or spatially limited (29), or lacked lithologic (30, 31), or paleogeographic con-  
80 text (32, 33). We quantify the contribution from carbonate and siliciclastic sediment loading on  
81 accommodation using a North America-specific dataset and consider implications for continen-

82 tal flooding and the termination of the Great Unconformity. We present a conceptual model that  
83 links observed changes in preserved carbonate rock volumes to the advent of carbonate biomin-  
84 eralization. We conclude with predictions for the carbon cycle and climate from our model of a  
85 time-varying continental carbonate rock reservoir.

86 **The continental carbonate rock reservoir increased in the early Paleozoic** To estimate  
87 changes in the size of the continental carbonate rock reservoir through time, we used global  
88 and regional geologic maps to tabulate the area of siliciclastic, carbonate, and mixed carbonate-  
89 siliciclastic sedimentary rocks through time. Results of this tabulation are explored as area,  
90 area/Ma, binned fraction of each sediment type, and binned fraction of all sediment types (Fig.  
91 1,S1,S2,S3,S4). When area is binned by paleolatitude, carbonates and mixed systems invari-  
92 ably tend to form in equatorial regions (Fig. 1C). Despite significant equatorial continental  
93 landmasses in the Neoproterozoic, carbonates are not a dominant sediment type until the Cam-  
94 brian (Cm, 538.8–485.4 Ma, Fig. 1). Neoproterozoic equatorial mixed carbonate-siliciclastic  
95 sediment deposits are preserved even when carbonate deposits are not (Fig. 1C, Movie S1).  
96 The Cretaceous and early Phanerozoic have the largest area of carbonate rocks, reflecting pe-  
97 riods of continental inundation (See probability density functions in Fig. 1C, K and Cm–O,  
98 respectively). There is a ~175% increase in total carbonate area across the Neoproterozoic–  
99 Phanerozoic transition (Fig. S1). While the global increase in binned area appears abrupt, it is  
100 more likely that there is a gradual increase in carbonate rock area observed across the Cambrian  
101 and Ordovician similar to what is observed in the higher resolution North American Macrostrat  
102 database. A gradual increase would likely reflect long-lived transgression and relative sea level  
103 rise associated with the termination of the Great Unconformity (see Fig. 1G (solid blue line),  
104 2, 3) (29). Siliciclastic rocks dominate in mid-latitudes through time and decrease in area by  
105 ~15% across the Neoproterozoic–Phanerozoic transition (Fig. S1).

106 We also see striking differences in the preserved sedimentary record of each continent (Fig.  
107 S3,S4). The increase in carbonate area in the early Phanerozoic is concentrated on four paleo-  
108 equatorial landmasses: North America, Siberia, North China, and South China (Fig. 2A, Figs.  
109 S3,S4,S5,S6, Movie S1). Conversely, continents at higher paleo-latitudes do not show this in-  
110 crease. These results are based on surface exposures on each continent with differences in  
111 mapping resolution. A next step would combine continent scale surface observations with sub-  
112 surface constraints as has been done in North America (29).

113 Erosion is an undeniable control on the preserved rock record and is commonly invoked  
114 to explain temporal changes in the volume of sedimentary rocks, yet predictions from erosion-  
115 dominated models do not fit the preserved carbonate and siliciclastic patterns. To assess whether  
116 the early Phanerozoic increase in carbonate rocks can be explained solely by erosive processes,  
117 we compare preservation patterns in carbonate and siliciclastic rocks, assuming that erosion  
118 will have affected both in similar ways. Results are reported as binned proportions defined as  
119 the area of a given rock type preserved during an interval of time divided by the total area of  
120 that rock type summed across the entire rock record (Figure 1D,E). The fraction of the total  
121 carbonate rock area within four time bins makes distinct, stepwise changes while the fraction  
122 of the total siliciclastic area within four time bins monotonically increases towards the modern  
123 (Fig. 1D,E, bins are 2500–538.8, 538.8–358.9, 358.9–145, 145–0 Ma). The four time bins  
124 represent 43%, 3.9%, 4.7%, and 3.2% of Earth history, respectively. Another way to assess  
125 erosional biases is to consider the proportion of carbonate rocks to all sedimentary rocks at a  
126 given point in time. We compared estimates of the proportion of carbonate to all sedimentary  
127 rocks from four datasets relevant to the continental rock reservoir (Fig. 1F). These four datasets  
128 suggest carbonate rocks increase from ~10–20% of all rock types in the Neoproterozoic to  
129 ~30–70% of all rock types in early Phanerozoic rocks, depending on the data source (Fig. 1F).

130 For comparison, we also calculated the proportion of deep-sea carbonates to all deep-sea sed-  
131 iments since the Jurassic using three available compilations. Even if erosion has removed a  
132 Proterozoic continental carbonate rock reservoir that rivaled today's (i.e., during the Grenville  
133 Orogeny (34), the first Neoproterozoic Snowball Earth glaciation (2, 35), or the younger Pan-  
134 African and Trans-Antarctic Orogenies (36)), our results require that carbonates would have  
135 been selectively removed relative to other Proterozoic sediments. Furthermore, Mesoprotero-  
136 zoic and early Neoproterozoic erosive events would still leave more than a hundred million  
137 years (650–~500 Ma) without a large continental carbonate rock reservoir and the growth of  
138 the reservoir in the early Phanerozoic would remain consequential for carbon sequestration dy-  
139 namics.

140 Geodynamic triggers must also be considered as possible drivers of the observed continen-  
141 tal carbonate reservoir signature. Tectonically driven continental emergence can be linked to  
142 enhanced weathering of continental crust and increased oceanic alkalinity, favoring carbonate  
143 precipitation. Proposed tectonic triggers for emergence or flooding include 1) shifting global  
144 tectonothermal stages (e.g. (37, 38)), 2) secular cooling of the Earth (e.g. (39)), and 3) regional  
145 tectonic events, all of which make testable predictions. A tectonothermal shift from hot, thin  
146 crust and low orogens spanning from 2000 Ma-800 Ma, to thick, cool crust and modern orogenic  
147 styles after 800 Ma is consistent with some datasets (dT/dP and zircon distributions) (38, 40, 41);  
148 a Neoproterozoic shift in crustal thickness could impact continental freeboard and weather-  
149 ing (37). Alternatively, global models of Earth's secular cooling predict the emergence of  
150 continents and coeval acceleration of continental weathering (e.g. (39, 42, 43)); recent mod-  
151 eling suggests that large-scale emergence transpired over a 100-300 Ma window, most likely in  
152 the Neoproterozoic ~700 Ma (39). If current models of either a tectonothermal shift or sec-  
153 ular cooling are correct, the timing of tectonic emergence and weathering would predate the

154 transformation of carbonate deposition by as much as 300 Ma (38, 39, 41), although evolving  
155 research may add further insights (e.g. (39, 40)). In addition to perturbing global weathering,  
156 this emergence is predicted to shift the locus of shallow marine carbonate precipitation from  
157 intercontinental seas to narrow ribbons of continental shelves (39). This prediction is at odds  
158 with the dataset we present here—moving carbonate precipitation to narrow continental shelves  
159 would likely not increase the area and volume of carbonate sediment in the early Phanerozoic.  
160 Buoyant young oceanic crust associated with the breakup of Rodinia has also been suggested as  
161 a global driver of early Paleozoic continental flooding, however this fails to match the evidence  
162 in our tabulation of equator-dominated flooding and instead would predict latitude-agnostic  
163 flooding (44). The observed increase in both carbonate and siliciclastic sediment area across all  
164 latitudes in the Cretaceous more closely matches the prediction from accommodation increase  
165 driven by buoyant young oceanic crust(Fig. 1C).

166 Regional tectonic events may also act as first-order controls on geochemical cycles and con-  
167 tinental emergence or flooding (e.g. (45)), yet also poorly explain the temporal, continent-  
168 specific, lithologic patterns documented above. Proposed regional tectonic models of global  
169 weathering and emergence or flooding include uplift associated with diachronous Neoprotero-  
170 zoic superplume upwelling and rifting (34, 35, 46–49), Ediacaran-Cambrian rifting (50), or  
171 Pan-African (650–500 Ma) and Transantarctic orogenies (615–470 Ma) (36, 51, 52). Most of  
172 these regional tectonic events significantly predate the Neoproterozoic-Phanerozoic transition  
173 (e.g. (34, 36, 50, 52–54)). While the Pan-African and Transantarctic orogenies coincide in time,  
174 their influences likely dominate on continents not characterized by the most significant early Pa-  
175 leozoic flooding and carbonate deposition. If orogeny-driven weathering was solely responsible  
176 for the early Paleozoic carbonate signal, both siliciclastic and carbonate depositional systems  
177 should be affected, yet our datasets indicate a dramatic increase in the carbonate rock reservoir

178 across the early Paleozoic, with no comparable pattern in the siliciclastic reservoir. Regional  
179 transformations of continental margins from ‘rift to drift’ along with thermal subsidence have  
180 been suggested as important controls on the early Paleozoic flooding signature in North Amer-  
181 ica (55) despite distinct, margin-specific rifting timescales. While any of the above geodynamic  
182 paradigms may correctly explain geochemical signals consistent with higher alkalinity by the  
183 end of the Proterozoic, a potential precondition for biomineralization (i.e.  $^{87}\text{Sr}/^{86}\text{Sr}$ ) (48,56,57),  
184 the temporal constraints and and locus of carbonate-dominated deposition in the tropics cap-  
185 tured in our datasets in the early Paleozoic are not fully consistent with tectonic predictions.

### 186 **Carbonate-driven crustal loading feedback contributes to growth of carbonate reservoir**

187 Relative sea-level rise across the Neoproterozoic–Phanerozoic transition inundated many con-  
188 tinental interiors after a long period of erosion or non-deposition, terminating the Great Uncon-  
189 formity (1, 2). Using a dataset currently only available for North America that includes age,  
190 thickness, and areal extent of surface and subsurface rocks (29), we first explore the variability  
191 of sediment load by creating cross sections of the continent showing both thickness and age of  
192 all rock units (i.e., a Wheeler Diagram)(Fig. 2B, Fig. S7) (29). The continental margins have  
193 thicker deposits of both siliciclastics and carbonates (Fig. 2B, Fig. S7). The continental interior  
194 has thinner sedimentary units that are primarily carbonate from ~500–420 Ma. The sedimen-  
195 tation dataset is used as an input into a gravitationally self-consistent calculation of relative  
196 sea level change (or accommodation) across the Neoproterozoic–Phanerozoic boundary(Fig. 3,  
197 Figs. S8,S9,S10,S11) (58). Given uncertainties in reconstructing lithospheric thickness and  
198 mantle rheologies in the Cambrian, we use estimates for a modern North American lithosphere  
199 and mantle configuration (59).

200 Our analysis highlights clear lithology-specific differences in the locus and style of sediment  
201 loading; accommodation from carbonate loading is continent-wide in the early Phanerozoic

202 and siliciclastic loading is concentrated in tectonic basins (Fig. 3). From 600–540 Ma, ac-  
203 commodation from carbonate loading ( $<600$  m/10 Myr) is limited to the western and northern  
204 North American margins (paleo-northern and eastern respectively). After the Neoproterozoic-  
205 Phanerozoic boundary, much of North America experienced 200–1200 m/10 Myr of accom-  
206 modation from carbonate sediment loading (Fig. 3). Relative sea-level rise from carbonate  
207 loading is highest in the Middle to Late Ordovician with  $\sim 1200$  meters/10 Myr predicted along  
208 the (present-day) western margin (460–450 Ma, Fig. 3). Carbonate-induced subsidence de-  
209 creases significantly across North America associated with and following the end-Ordovician  
210 glaciation (Fig. S10) (60). In contrast to the pattern of widespread crustal subsidence associ-  
211 ated with carbonate deposition, siliciclastic loading is concentrated within tectonically active  
212 basins like the Taconic foreland basin along the modern eastern margin of North America (Figs.  
213 S8,S9,S10,S11). Maximum siliciclastic-induced loading is also similar between Ediacaran and  
214 early Paleozoic basins (Figs. S8,S9,S10,S11).

215 Nearshore sediment loading and an increase in accommodation associated with productive,  
216 voluminous, tropical carbonate platforms could represent a positive feedback on continent-scale  
217 flooding by expanding available shallow marine environments for new carbonate sedimentation.  
218 A subsidence feedback from carbonate sedimentation could explain early Paleozoic flooding far  
219 into continental interiors and amplify any potential tectonic or glacio-eustatic drivers of relative  
220 sea-level rise in the Cambrian and Ordovician (Fig. 1, Cm and O on timescale, respectively) (2).  
221 From our analysis of global time-constrained lithologic maps (58), we observe that the cratons  
222 with the largest sediment signal of early Phanerozoic flooding were in the tropics and accumu-  
223 lating carbonate (i.e., North America, and the Siberian, North, and South China cratons)(Figs.  
224 S3,S4,S5,S6, Movie S1). Although carbonate sediment area increased substantially on these  
225 continents, siliciclastic sediment area and proportion did not increase from the Proterozoic to

226 Phanerozoic on almost all continents (Figs. S1,S3,S4). This pattern argues against a global  
227 cause of extreme sea-level rise and highlights that a defining feature of the Great Unconformity  
228 may be synchronous tropical flooding. Tectonic drivers may be fundamentally important for  
229 shifting sea water chemistry and nutrient fluxes in the Late Neoproterozoic (56, 57), yet the  
230 inconsistencies between predictions from existing tectonic frameworks or erosion and our re-  
231 sults, including sedimentation patterns and loading dynamics, necessitates a more innovative  
232 interpretation of the carbonate system.

233 **Conceptual Model** The early Phanerozoic increase in carbonate areal extent and volume in  
234 proportion to other sediments combined with our accommodation modeling, lead us to pro-  
235 pose a conceptual model to explain carbonate reservoir changes across the Neoproterozoic–  
236 Phanerozoic transition. We hypothesize that evolutionary innovations of carbonate biomin-  
237 eralization in organisms in shallow carbonate platforms led to more productive and volumi-  
238 nous carbonate depositional environments with significant progradation (the seaward growth of  
239 carbonate platforms). The emergence and expansion of carbonate biomineralization spanned  
240 eukaryotic (animal, algal, and protistan) clades and was associated with biochemical, cel-  
241 lular, metabolic, tissual, anatomical, and habitat-scale innovations (61). By the latest Pro-  
242 terozoic, biomineralizing organisms evolved mechanisms to overcome kinetic inhibition us-  
243 ing membrane-bound pumps that increase the Ca/Mg ratio and pH at the site of calcification,  
244 as well as enzymes like carbonic anhydrase, that ultimately boost precipitation rate (62). A  
245 gradual transformation of the nearshore carbonate factory to one dominated by biomineralizers  
246 occurred over the Cambrian Explosion and Great Ordovician Biodiversification event (63)(Fig.  
247 4B,C). The growth of the early Paleozoic continental carbonate rock reservoir was a function of  
248 both an increase in carbonate production and a positive feedback between efficient biologically-  
249 mediated carbonate production, progradation, and subsidence, together enhancing carbon se-

250 questration on continental crust (Fig. 4B,C).

251 By contrast, kinetic and physical inhibitors must have slowed precipitation and ultimately  
252 limited production volumes in Proterozoic microbe-dominated reefs. Proterozoic carbonate  
253 platforms are primarily dolomite ( $\text{CaMg}(\text{CO}_3)_2$ ) and much of it likely formed slowly at or near  
254 the seafloor( (64) and references therein). The rock record suggests that without the advantages  
255 of biomineralization,  $\text{Mg}^{2+}$  inhibited carbonate precipitation rates, forcing proto-dolomite or  
256 dolomite precipitation in shallow water environments. Trace elements and phosphate have also  
257 been invoked as important Proterozoic carbonate kinetic inhibitors at key intervals (65, 66).  
258 Siliciclastics, like those often found interbedded with Proterozoic shallow water dolomite and  
259 deeper water limestone, could have also physically inhibited carbonate precipitation before  
260 biomineralizing organisms could construct voluminous reefs far from siliciclastic depocenters  
261 (Fig. 4). Less voluminous Proterozoic platforms would have a limited positive feedback on  
262 subsidence and regional sea-level trends—despite aggrading to sea-level and having similar  
263 platform architectures (67).

264 Biomineralizing animals and algae may have increased the range of environments of carbon-  
265 ate deposition in the early Paleozoic, but more importantly our results suggest biominerals in  
266 combination with a feedback on subsidence increased the total volume of carbonate deposited  
267 on continental crust, perhaps taking advantage of a recently created Neoproterozoic alkalinity  
268 reservoir (56, 57). Building a large early Paleozoic continental carbonate rock reservoir would  
269 have ramifications for the long-term carbon cycle and climate.

270 **Predictions for the Carbon Cycle and Climate** In the Precambrian a smaller, more sluggish  
271 long-term flux into shallow marine carbonate platforms and a smaller continental carbonate  
272 reservoir require other changes in the carbon cycle and weathering to maintain quasi-steady

273 state over long geologic timescales (14). While abiotic processes that add carbonate to the deep  
274 sea may have been locally important in the Proterozoic, including water column and seafloor  
275 precipitates (68), offshore transport of carbonate sediments, and carbonate precipitation associ-  
276 ated with serpentinization, we suggest it is unlikely that they would equal the combined sizes  
277 of the large continental and deep sea carbonate rock reservoirs we have today (15, 20, 69–71).  
278 A small deep sea reservoir would imply that the return carbon flux into the mantle during the  
279 Precambrian was smaller than today, perhaps resulting in lower volcanic CO<sub>2</sub> outgassing rates  
280 despite Earth's warmer interior temperature (Fig. 4A). A deep sea carbonate reservoir smaller  
281 than the recent (145–0 Ma) would also not have been able to buffer the carbon cycle during  
282 climatic events in the same way it does today (72). We estimate inorganic carbon burial flux on  
283 continental crust (margins and inland seas) through time (Fig. S2A) despite the imperfect nature  
284 of the preserved record (71) and compare it to estimates of the recent deep sea burial flux (Fig.  
285 S2A). We consider the impact of a smaller carbonate burial flux on inorganic carbon residence  
286 time using the modern size of the DIC reservoir over the entire time interval (38973 GtC) or a  
287 larger reservoir in the Precambrian and early Paleozoic (101000 GtC) (73). Estimated residence  
288 times increase to 1–2.5 million years in the Precambrian if one assumes carbonate platforms on  
289 continental crust are the dominant carbonate sequestering environment before the evolution of  
290 planktonic calcifying organisms (Fig. S2B). The unique aspects of the Neoproterozoic carbon  
291 cycle proposed here (i.e. smaller continental and deep sea carbonate rock reservoirs, sluggish  
292 carbon sequestration into microbial and abiotic carbonates, and a gradual increase in alkalinity  
293 influx due to tectonic and climatic changes in the Neoproterozoic) may have created differ-  
294 ent internal dynamics during Neoproterozoic carbon cycle perturbations as evidenced by larger  
295 magnitude, longer-lived, carbon isotope excursions in shallow water platform environments  
296 (Fig. 1A). In the Phanerozoic both the Cambrian and early Triassic periods are dominated by  
297 abiotic and microbial carbonates, high DIC, and high pCO<sub>2</sub> (Fig. 1, Cm and Tr on timescale,

298 respectively). These two time intervals have some of the most extreme carbon isotope pertur-  
299 bations of the Phanerozoic suggesting similar internal feedbacks as the Neoproterozoic (Fig.  
300 1A).

301 Organic carbon burial, another critical sink of Earth's carbon cycle, could increase alongside  
302 carbonate burial in the early Paleozoic ( $f_{org}$ ) maintaining long-term carbon isotopic composi-  
303 tions (74). Multiple models have considered a larger Neoproterozoic dissolved organic carbon  
304 pool (75, 76). If carbonate loading flooded tropical continents, organic carbon could have been  
305 sequestered along with carbonate rocks. This is consistent with evidence that organic carbon  
306 burial increased in the sedimentary rocks overlying the Great Unconformity (77). By aiding in  
307 organic carbon burial, carbonate biomineralization would play a role in increasing atmospheric  
308  $O_2$ .

309 Under the model proposed here (Fig. 4),  $CO_2$  sequestration into voluminous continental  
310 carbonates during the early Phanerozoic would shrink the size of the ocean [DIC] reservoir  
311 and ultimately atmosphere  $CO_2$ , driving cooling. Long-term cooling is consistent with the  
312 interpretation that temperature is the primary control on the observed  $\delta^{18}O$  increase in well-  
313 preserved Paleozoic fossils (5–8), and is supported by carbonate clumped isotope temperatures  
314 across the early Phanerozoic (4)(Fig. 1B). From independent constraints,  $pCO_2$  is also predicted  
315 to fall over this time interval (78). Elevated temperatures in the Cambrian and early Ordovician,  
316 in combination with low dissolved oxygen (79), may have stressed early animals; our model of  
317 expanding carbonate platforms, ultimately lowering DIC and  $CO_2$ , and reducing temperature  
318 provides an avenue for relieving the thermal stress these organisms felt (79)(Fig. 1, Cm and  
319 O on timescale, respectively). Coupled with enhanced weathering in the Neoproterozoic (47,  
320 48, 56) and middle to late Ordovician tectonic changes (10, 80–82), a biomineralization-driven  
321 growth in the carbonate continental rock reservoir could have ultimately helped to cool the

322 planet leading into the end-Ordovician glaciation by reducing the size of the DIC reservoir.

323 **Conclusions** Evolutionary-led changes to the carbon cycle are fundamental to our interpreta-  
324 tions of Earth's past climate and environments and to our understanding of the co-evolution of  
325 life and our planet. We present evidence that early Phanerozoic shallow water carbonate reefs  
326 were voluminous and drove crustal loading and accommodation increase in the tropics, ending  
327 the Great Unconformity. Our results underscore an interplay between biomineralization and  
328 geodynamics, where efficient carbonate precipitation is actively driving basin development in  
329 regions with low relief. This biomineralization-driven change, in addition to others including  
330 the evolution of planktonic biomineralization, have the power to influence not just the surface  
331 on Earth but also its interior, requiring non-uniformitarian interpretations of carbon cycle reser-  
332 voirs and fluxes, including volcanic outgassing.

## References and Notes

1. S. E. Peters, R. R. Gaines, Formation of the 'Great Unconformity' as a trigger for the Cambrian explosion. *Nature* **484**, 363–6 (2012).
2. C. Brenhin Keller, J. M. Husson, R. N. Mitchell, W. F. Bottke, T. M. Gernon, P. Boehnke, E. A. Bell, N. L. Swanson-Hysell, S. E. Peters, Neoproterozoic glacial origin of the Great Unconformity. *Proc. Natl. Acad. Sci. U. S. A.* **116**, 1136–1145 (2019).
3. M. R. Saltzman, E. Thomas, Carbon Isotope Stratigraphy. *Geol. Time Scale 2012* **1-2**, 207–232 (2012).
4. K. Bergmann, S. Finnegan, R. Creel, J. Eiler, N. Hughes, L. Popov, W. Fischer, A paired apatite and calcite clumped isotope thermometry approach to estimating Cambro-Ordovician seawater temperatures and isotopic composition. *Geochim. Cosmochim. Acta* **224** (2018).
5. J. A. Trotter, I. S. Williams, C. R. Barnes, C. Lécuyer, R. S. Nicoll, Did cooling oceans trigger Ordovician biodiversification? Evidence from conodont thermometry. *Science* **321**, 550–554 (2008).
6. S. L. Goldberg, T. M. Present, S. Finnegan, K. D. Bergmann, A high-resolution record of early Paleozoic climate. *Proceedings of the National Academy of Sciences* **118** (2021).
7. J. Veizer, P. Bruckschen, F. Pawellek, A. Diener, O. G. Podlaha, G. A. F. Carden, T. Jasper, C. Korte, H. Strauss, K. Azmy, D. Ala, Oxygen isotope evolution of Phanerozoic seawater. *Palaeogeogr. Palaeoclimatol. Palaeoecol.* **132**, 159–172 (1997).
8. E. Grossman, M. Joachimski, Oxygen isotope stratigraphy. *Geologic Time Scale 2020* (Elsevier, 2020), pp. 279–307.

- 355 9. F. A. Macdonald, R. Wordsworth, Initiation of Snowball Earth with volcanic sulfur aerosol  
356 emissions. *Geophys. Res. Lett.* **44**, 1938–1946 (2017).
- 357 10. F. A. Macdonald, N. L. Swanson-Hysell, Y. Park, L. Lisiecki, O. Jagoutz, Arc-continent  
358 collisions in the tropics set Earth’s climate state. *Science* (80-. ). **364**, 181–184 (2019).
- 359 11. P. F. Hoffman, D. S. Abbot, Y. Ashkenazy, D. I. Benn, J. J. Brocks, P. A. Cohen, G. M.  
360 Cox, J. R. Creveling, Y. Donnadieu, D. H. Erwin, I. J. Fairchild, D. Ferreira, J. C. Good-  
361 man, G. P. Halverson, M. F. Jansen, G. Le Hir, G. D. Love, F. A. Macdonald, A. C. Maloof,  
362 C. A. Partin, G. Ramstein, B. E. Rose, C. V. Rose, P. M. Sadler, E. Tziperman, A. Voigt,  
363 S. G. Warren, Snowball Earth climate dynamics and Cryogenian geology-geobiology. *Sci.*  
364 *Adv.* **3** (2017).
- 365 12. P. F. Hoffman, The Great Oxidation Event and a Siderian Snowball Earth: MIF based  
366 correlation of Paleoproterozoic glaciations. *Chem. Geol.* (2013).
- 367 13. J. C. Walker, P. B. Hays, J. F. Kasting, A negative feedback mechanism for the long-term  
368 stabilization of Earth’s surface temperature. *J. Geophys. Res.* **86**, 9776–9782 (1981).
- 369 14. T. T. Isson, N. J. Planavsky, Reverse weathering as a long-term stabilizer of marine pH  
370 and planetary climate. *Nature* **560**, 471–475 (2018).
- 371 15. A. Ridgwell, R. E. Zeebe, The role of the global carbonate cycle in the regulation and  
372 evolution of the Earth system. *Earth Planet. Sci. Lett.* **234**, 299–315 (2005).
- 373 16. T. T. Isson, N. J. Planavsky, L. Coogan, E. Stewart, J. Ague, E. Bolton, S. Zhang,  
374 N. McKenzie, L. Kump, Evolution of the global carbon cycle and climate regulation on  
375 earth. *Global Biogeochemical Cycles* **34**, e2018GB006061 (2020).

- 376 17. T. W. Dahl, S. K. Arens, The impacts of land plant evolution on Earth's climate and  
377 oxygenation state—An interdisciplinary review. *Chemical Geology* **547**, 119665 (2020).
- 378 18. A. J. Fraass, D. C. Kelly, S. E. Peters, Macroevolutionary History of the Planktic  
379 Foraminifera. *Annu. Rev. Earth Planet. Sci.* **43**, 139–166 (2015).
- 380 19. P. R. Bown, J. A. Lees, J. R. Young, Calcareous nannoplankton evolution and diversity  
381 through time. *Coccolithophores* (Springer, 2004), pp. 481–508.
- 382 20. J. M. Edmond, Y. Huh, Non-steady state carbonate recycling and implications for the  
383 evolution of atmospheric pCO<sub>2</sub>. *Earth Planet. Sci. Lett.* **216**, 125–139 (2003).
- 384 21. R. S. Arvidson, F. T. Mackenzie, R. A. Berner, F. T. Mackenzie, R. A. Berner, The Sensi-  
385 tivity of the Phanerozoic Inorganic Carbon System to the Onset of Pelagic Sedimentation.  
386 *Aquat Geochem* **20**, 343–362 (2014).
- 387 22. B. H. Wilkinson, Biomineralization, paleoceanography, and the evolution of calcareous  
388 marine organisms. *Geology* **7**, 524 (1979).
- 389 23. R. S. Arvidson, F. T. Mackenzie, M. Guidry, Magic: A phanerozoic model for the geo-  
390 chemical cycling of major rock-forming components. *American Journal of Science* **306**,  
391 135–190 (2006).
- 392 24. R. A. Berner, F. T. Mackenzie, Burial and Preservation of Carbonate Rocks Over Phanero-  
393 zoic Time. *Aquat. Geochemistry* **17**, 727–733 (2011).
- 394 25. F. T. Mackenzie, J. W. Morse, Sedimentary carbonates through Phanerozoic time.  
395 *Geochim. Cosmochim. Acta* **56**, 3281–3295 (1992).
- 396 26. L. J. Walker, B. H. Wilkinson, L. C. Ivany, Continental Drift and Phanerozoic Carbonate  
397 Accumulation in Shallow-Shelf and Deep-Marine Settings. *J. Geol.* **110**, 75–87 (2002).

- 398 27. B. H. Wilkinson, T. J. Algeo, Sedimentary carbonate record of calciummagnesium cy-  
399 cling. *Am. J. Sci.* **289**, 1158–1194 (1989).
- 400 28. B. H. Wilkinson, B. N. Opdyke, T. J. Algeo, Time partitioning in cratonic carbonate rocks.  
401 *Geology* **19**, 1093–1096 (1991).
- 402 29. S. E. Peters, J. M. Husson, J. Czaplewski, Macrostrat: a platform for geological data  
403 integration and deep-time earth crust research. *Geochemistry, Geophysics, Geosystems*  
404 **19**, 1393–1409 (2018).
- 405 30. B. H. Wilkinson, B. J. McElroy, S. E. Kesler, S. E. Peters, E. D. Rothman, Global geologic  
406 maps are tectonic speedometers - Rates of rock cycling from area-age frequencies. *Bull.*  
407 *Geol. Soc. Am.* **121**, 760–779 (2009).
- 408 31. S. E. Peters, J. M. Husson, Sediment cycling on continental and oceanic crust. *Geology*  
409 **45**, 323–326 (2017).
- 410 32. A. B. Ronov, V. E. Khain, A. N. Balukhovskiy, K. B. Seslavinsky, Quantitative analysis of  
411 Phanerozoic sedimentation. *Sediment. Geol.* **25**, 311–325 (1980).
- 412 33. W. W. Hay, Carbonate sedimentation through the late precambrian and phanerozoic. *Zen-*  
413 *tralblatt für Geologie und Paläontologie/Teil 1* **1998**, 435–445 (1999).
- 414 34. R. M. Flowers, F. A. Macdonald, C. S. Siddoway, R. Havranek, Diachronous development  
415 of great unconformities before neoproterozoic snowball earth. *Proceedings of the National*  
416 *Academy of Sciences* **117**, 10172–10180 (2020).
- 417 35. M. DeLucia, W. R. Guenther, S. Marshak, S. Thomson, A. Ault, Thermochronology links  
418 denudation of the great unconformity surface to the supercontinent cycle and snowball  
419 earth. *Geology* **46**, 167–170 (2018).

- 420 36. R. J. Squire, I. H. Campbell, C. M. Allen, C. J. Wilson, Did the Transgondwanan Super-  
421 mountain trigger the explosive radiation of animals on Earth? *Earth Planet. Sci. Lett.* **250**,  
422 116–133 (2006).
- 423 37. E. Moores, Neoproterozoic oceanic crustal thinning, emergence of continents, and origin  
424 of the phanerozoic ecosystem: A model. *Geology* **21**, 5–8 (1993).
- 425 38. C. J. Spencer, R. N. Mitchell, M. Brown, Enigmatic mid-proterozoic orogens: Hot, thin,  
426 and low. *Geophysical Research Letters* **48**, e2021GL093312 (2021).
- 427 39. C.-T. A. Lee, J. Caves, H. Jiang, W. Cao, A. Lenardic, N. R. McKenzie, O. Shorttle, Q.-z.  
428 Yin, B. Dyer, Deep mantle roots and continental emergence: Implications for whole-earth  
429 elemental cycling, long-term climate, and the cambrian explosion. *International Geology*  
430 *Review* **60**, 431–448 (2018).
- 431 40. M. Brown, C. Kirkland, T. Johnson, Evolution of geodynamics since the archean: Signif-  
432 icant change at the dawn of the phanerozoic. *Geology* **48**, 488–492 (2020).
- 433 41. C. J. Spencer, Continuous continental growth as constrained by the sedimentary record.  
434 *American Journal of Science* **320**, 373–401 (2020).
- 435 42. N. Vlaar, Continental emergence and growth on a cooling earth. *Tectonophysics* **322**,  
436 191–202 (2000).
- 437 43. N. Flament, N. Coltice, P. F. Rey, A case for late-Archaeon continental emergence from  
438 thermal evolution models and hypsometry. *Earth Planet. Sci. Lett.* **275**, 326–336 (2008).
- 439 44. G. C. Bond, P. A. Nickeson, M. A. Kominz, Breakup of a supercontinent between 625 Ma  
440 and 555 Ma: new evidence and implications for continental histories. *Earth Planet. Sci.*  
441 *Lett.* **70**, 325–345 (1984).

- 442 45. K. Sundell, F. Macdonald, The tectonic context of hafnium isotopes in zircon. *Earth and*  
443 *Planetary Science Letters* **584**, 117426 (2022).
- 444 46. F. Horton, Did phosphorus derived from the weathering of large igneous provinces fertilize  
445 the neoproterozoic ocean? *Geochemistry, Geophysics, Geosystems* **16**, 1723–1738 (2015).
- 446 47. Y. Godd eris, Y. Donnadi eu, A. N ed elec, B. Dupr e, C. Dessert, A. Grard, G. Ramstein,  
447 L. M. Fran ois, The Sturtian 'snowball' glaciation: Fire and ice. *Earth Planet. Sci. Lett.*  
448 **211**, 1–12 (2003).
- 449 48. G. M. Cox, G. P. Halverson, R. K. Stevenson, M. Vokaty, A. Poirier, M. Kunzmann, Z. X.  
450 Li, S. W. Denyszyn, J. V. Strauss, F. A. Macdonald, Continental flood basalt weathering as  
451 a trigger for Neoproterozoic Snowball Earth. *Earth Planet. Sci. Lett.* **446**, 89–99 (2016).
- 452 49. Y. Godd eris, Y. Donnadi eu, S. Carretier, M. Aretz, G. Dera, M. MacOuin, V. Regard, On-  
453 set and ending of the late Palaeozoic ice age triggered by tectonically paced rock weath-  
454 ering. *Nat. Geosci.* **10**, 382–386 (2017).
- 455 50. B. Robert, M. Domeier, J. Jakob, On the origins of the Iapetus ocean. *Earth-Science*  
456 *Reviews* **221**, 103791 (2021).
- 457 51. Z. Zhu, I. H. Campbell, C. M. Allen, J. J. Brocks, B. Chen, The temporal distribution  
458 of earth's supermountains and their potential link to the rise of atmospheric oxygen and  
459 biological evolution. *Earth and Planetary Science Letters* **580**, 117391 (2022).
- 460 52. J. G. Meert, B. S. Lieberman, The Neoproterozoic assembly of Gondwana and its rela-  
461 tionship to the Ediacaran-Cambrian radiation. *Gondwana Res.* **14**, 5–21 (2008).
- 462 53. D. C. Bradley, Passive margins through earth history. *Earth-Science Rev.* **91**, 1–26 (2008).
- 463 54. D. C. Bradley, Secular trends in the geologic record and the supercontinent cycle (2011).

- 464 55. G. C. Bond, M. A. Kominz, M. S. Steckler, J. P. Grotzinger, Role of Thermal Subsidence,  
465 Flexure, and Eustasy in the Evolution of Early Paleozoic Passive-Margin Carbonate Plat-  
466 forms (1989).
- 467 56. S. T. Brennan, T. K. Lowenstein, J. Horita, Seawater chemistry and the advent of biocal-  
468 cification. *Geology* **321**, 473–476 (2004).
- 469 57. Y. Petrychenko, T. M. Peryt, E. I. Chechel, Early cambrian seawater chemistry from fluid  
470 inclusions in halite from siberian evaporites. *Chemical Geology* **219**, 149–161 (2005).
- 471 58. Materials and methods are available as supplementary materials at the science website .
- 472 59. N. Zhang, S. Zhong, W. Leng, Z.-X. Li, A model for the evolution of the earth's mantle  
473 structure since the early paleozoic. *Journal of Geophysical Research: Solid Earth* **115**  
474 (2010).
- 475 60. S. Finnegan, N. a. Heim, S. E. Peters, W. W. Fischer, Climate change and the selective  
476 signature of the Late Ordovician mass extinction. *Proc. Natl. Acad. Sci.* **109**, 6829–6834  
477 (2012).
- 478 61. P. U. Gilbert, K. D. Bergmann, N. Boekelheide, S. Tambutté, T. Mass, F. Marin, J. F. Ad-  
479 kins, J. Erez, B. Gilbert, V. Knutson, M. Cantine, J. O. Hernández, A. H. Knoll, Biominer-  
480 alization: Integrating mechanism and evolutionary history. *Science Advances* **8**, eabl9653  
481 (2022).
- 482 62. T. Mass, A. J. Giuffre, C.-Y. Sun, C. A. Stifler, M. J. Frazier, M. Neder, N. Tamura, C. V.  
483 Stan, M. A. Marcus, P. U. P. A. Gilbert, Amorphous calcium carbonate particles form  
484 coral skeletons. *Proc. Natl. Acad. Sci. U. S. A.* **114**, E7670–E7678 (2017).

- 485 63. S. B. Pruss, S. Finnegan, W. W. Fischer, A. H. Knoll, Carbonates in skeleton-poor seas:  
486 New insights from Cambrian and Ordovician strata of Laurentia. *Palaios* **25**, 73–84  
487 (2010).
- 488 64. M. D. Cantine, A. H. Knoll, K. D. Bergmann, Carbonates before skeletons: A database  
489 approach. *Earth-Science Reviews* **201**, 103065 (2020).
- 490 65. D. Y. Sumner, J. P. Grotzinger, Were kinetics of Archean calcium carbonate precipitation  
491 related to oxygen concentration? *Geology* **24**, 119–122 (1996).
- 492 66. S. Roest-Ellis, J. V. Strauss, N. J. Tosca, Experimental constraints on nonskeletal CaCO<sub>3</sub>  
493 precipitation from Proterozoic seawater. *Geology* **49**, 561–565 (2021).
- 494 67. J. P. Grotzinger, Facies and evolution of Precambrian carbonate depositional systems:  
495 emergence of the modern platform archetype. *Control. carbonate Platf. basin Dev.* pp.  
496 71–106 (1989).
- 497 68. J. A. Higgins, W. W. Fischer, D. P. Schrag, Oxygenation of the ocean and sediments:  
498 Consequences for the seafloor carbonate factory. *Earth Planet. Sci. Lett.* **284**, 25–33  
499 (2009).
- 500 69. H. Pälike, *et al.*, A Cenozoic record of the equatorial Pacific carbonate compensation  
501 depth. *Nature* **488**, 609–614 (2012).
- 502 70. A. Paytan, E. M. Griffith, A. Eisenhauer, M. P. Hain, K. Wallmann, A. Ridgwell, A 35-  
503 million-year record of seawater stable sr isotopes reveals a fluctuating global carbon cycle.  
504 *Science* **371**, 1346–1350 (2021).
- 505 71. W. W. Hay, Carbonate fluxes and calcareous nannoplankton, *Tech. rep.* (2004).

- 506 72. A. J. Ridgwell, Carbonate Deposition, Climate Stability, and Neoproterozoic Ice Ages.  
507 *Science* (80-. ). **302**, 859–862 (2003).
- 508 73. D. E. Penman, A. D. Rooney, Coupled carbon and silica cycle perturbations during the  
509 marinoan snowball earth deglaciation. *Geology* **47**, 317–320 (2019).
- 510 74. J. M. Hayes, H. Strauss, A. J. Kaufman, The abundance of marine organic matter and  
511 isotopic fractionation in the global biogeochemical cycle of carbon during the past 800  
512 Ma. *Chem. Geol.* **161**, 103–125 (1999).
- 513 75. D. H. Rothman, J. M. Hayes, R. E. Summons, Dynamics of the Neoproterozoic carbon  
514 cycle. *Proc. Natl. Acad. Sci. USA* **100**, 8124–8129 (2003).
- 515 76. E. Tziperman, I. Halevy, D. T. Johnston, A. H. Knoll, D. P. Schrag, Biologically induced  
516 initiation of Neoproterozoic snowball-Earth events. *Proc. Natl. Acad. Sci. U. S. A.* **108**,  
517 15091–6 (2011).
- 518 77. J. M. Husson, S. E. Peters, Atmospheric oxygenation driven by unsteady growth of the  
519 continental sedimentary reservoir. *Earth Planet. Sci. Lett.* **460**, 68–75 (2017).
- 520 78. D. L. Royer, R. A. Berner, I. P. Montañez, N. J. Tabor, D. J. Beerling, CO<sub>2</sub> as a primary  
521 driver of Phanerozoic climate. *GSA Today* **14**, 4 (2004).
- 522 79. R. G. Stockey, A. Pohl, A. Ridgwell, S. Finnegan, E. A. Sperling, Decreasing Phanero-  
523 zoic extinction intensity as a consequence of Earth surface oxygenation and metazoan  
524 ecophysiology. *Proceedings of the National Academy of Sciences* **118** (2021).
- 525 80. O. Jagoutz, F. A. Macdonald, L. Royden, Low-latitude arc-continent collision as a driver  
526 for global cooling. *Proc. Natl. Acad. Sci. U. S. A.* **113**, 4935–4940 (2016).

- 527 81. S. M. Bergström, W. D. Huff, M. R. Saltzman, D. R. Kolata, S. A. Leslie, The Great-  
528 est Volcanic Ash Falls in the Phanerozoic: Trans-Atlantic Relations of the Ordovician  
529 Millbrig and Kinnekulle K-Bentonites. *Sediment. Rec.* **2**, 4–8 (2004).
- 530 82. S. A. Young, M. R. Saltzman, K. A. Foland, J. S. Linder, L. R. Kump, A major drop in  
531 seawater  $87\text{Sr}/86\text{Sr}$  during the Middle Ordovician (Darriwilian): Links to volcanism and  
532 climate? *Geology* **37**, 951–954 (2009).
- 533 83. Y. Park, N. L. Swanson-Hysell, S. A. MacLennan, A. C. Maloof, M. Gebreslassie, M. M.  
534 Tremblay, B. Schoene, M. Alene, E. S. Anttila, T. Tesema, B. Haileab, The lead-up to  
535 the Sturtian Snowball Earth: Neoproterozoic chemostratigraphy time-calibrated by the  
536 Tambien Group of Ethiopia. *GSA Bull.* **132**, 1119–1149 (2020).
- 537 84. v. d. S. B. F. J. M. C. A. C. G. Bachan, Aviv, J. L. Payne, Carbon cycle dynamics following  
538 the end-Triassic mass extinction: Constraints from paired  $\delta^{13}\text{C}_{carb}$  and  $\delta^{13}\text{C}_{org}$  records.  
539 *Geochemistry, Geophysics, Geosystems* **13** (2012).
- 540 85. A. C. Maloof, S. M. Porter, J. L. Moore, F. O. Dudas, S. A. Bowring, J. A. Higgins, D. A.  
541 Fike, M. P. Eddy, The earliest Cambrian record of animals and ocean geochemical change.  
542 *Geol. Soc. Am. Bull.* **122**, 1731–1774 (2010).
- 543 86. C. Yang, A. D. Rooney, D. J. Condon, X.-H. Li, D. V. Grazhdankin, F. T. Bowyer,  
544 C. Hu, F. A. Macdonald, M. Zhu, The tempo of Ediacaran evolution. *Science advances* **7**,  
545 eabi9643 (2021).
- 546 87. S.-T. Kim, J. R. O’Neil, Equilibrium and nonequilibrium oxygen isotope effects in syn-  
547 thetic carbonates. *Geochim. Cosmochim. Acta* **61**, 3461–3475 (1997).

- 548 88. J. Hartmann, N. Moosdorf, The new global lithological map database GLiM: A repre-  
549 sentation of rock properties at the Earth surface. *Geochemistry, Geophys. Geosystems* **13**  
550 (2012).
- 551 89. The data were downloaded from the EarthChem Portal on February 7, 2017, using the  
552 following parameters: rock classification = sedimentary, <http://portal.earthchem.org>.
- 553 90. S. E. Peters, M. McClennen, The Paleobiology Database application programming inter-  
554 face. *Paleobiology* **42**, 1–7 (2015).
- 555 91. F. M. Persits, T. S. Ahlbrandt, M. L. Tuttle, R. R. Charpentier, M. E. Brownfield, K. I.  
556 Takahashi, Maps showing geology, oil and gas fields and geological provinces of Africa,  
557 *Tech. rep.*, Reston, VA (1997).
- 558 92. R. M. Pollastro, A. S. Karshbaum, R. J. Viger, Maps showing geology, oil and gas fields  
559 and geologic provinces of the Arabian Peninsula, *Tech. rep.*, Reston, VA (1999).
- 560 93. F. Persits, G. Ulmishek, Maps showing geology, oil and gas fields, and geologic provinces  
561 of the Arctic, *Tech. rep.*, Reston, VA (2003).
- 562 94. D. W. Steinshouer, J. Qiang, P. J. McCabe, R. T. Ryder, Maps showing geology, oil and gas  
563 fields, and geologic provinces of the Asia Pacific region, *Tech. rep.*, Reston, VA (1999).
- 564 95. M. J. Pawlewicz, D. W. Steinshouer, D. L. Gautier, Map showing geology, oil and gas  
565 fields, and geologic provinces of Europe including Turkey, *Tech. rep.*, Reston, VA (2002).
- 566 96. R. M. Pollastro, F. M. Persits, D. W. Steinshouer, Maps showing geology, oil and gas  
567 fields, and geologic provinces of Iran, *Tech. rep.*, Reston, VA (1997).
- 568 97. C. P. Garrity, D. Soller, Database of the geologic map of North America— Adapted from  
569 the map by J.C. Reed, Jr. and others (2005), *Tech. rep.*, Reston, VA (2009).

- 570 98. C. J. Schenk, R. J. Viger, C. P. Anderson, Maps showing geology, oil and gas fields and  
571 geologic provinces of the South America region, *Tech. rep.*, Reston, VA (1999).
- 572 99. F. M. Persits, G. F. Ulmishek, D. W. Steinshouer, Maps showing geology, oil and gas fields  
573 and geologic provinces of the former Soviet Union, *Tech. rep.*, Reston, VA (1997).
- 574 100. A. S. Merdith, S. E. Williams, A. S. Collins, M. G. Tetley, J. A. Mulder, M. L. Blades,  
575 A. Young, S. E. Armistead, J. Cannon, S. Zahirovic, *et al.*, Extending full-plate tectonic  
576 models into deep time: Linking the Neoproterozoic and the Phanerozoic. *Earth-Science*  
577 *Reviews* **214**, 103477 (2021).
- 578 101. R. D. Müller, J. Cannon, X. Qin, R. J. Watson, M. Gurnis, S. Williams, T. Pfaffelmoser,  
579 M. Seton, S. H. Russell, S. Zahirovic, GPlates: building a virtual Earth through deep time.  
580 *Geochemistry, Geophysics, Geosystems* **19**, 2243–2261 (2018).
- 581 102. Z. X. Li, S. V. Bogdanova, A. S. Collins, A. Davidson, B. De Waele, R. E. Ernst, I. C. W.  
582 Fitzsimons, R. A. Fuck, D. P. Gladkochub, J. Jacobs, K. E. Karlstrom, S. Lu, L. M. Nat-  
583 apov, V. Pease, S. A. Pisarevsky, K. Thrane, V. Vernikovsky, Assembly, configuration, and  
584 break-up history of Rodinia: A synthesis. *Precambrian Research* **160**, 179–210 (2008).
- 585 103. A. Eyster, B. P. Weiss, K. Karlstrom, F. A. Macdonald, Paleomagnetism of the Chuar  
586 Group and evaluation of the late Tonian Laurentian apparent polar wander path with im-  
587 plications for the makeup and breakup of Rodinia. *Geological Society of America Bulletin*  
588 **132**, 710–738 (2020).
- 589 104. D. A. Evans, The palaeomagnetically viable, long-lived and all-inclusive Rodinia super-  
590 continent reconstruction. *Geological Society, London, Special Publications* **327**, 371–404  
591 (2009).

- 592 105. A. B. Ronov, V. Y. Khain, K. Seslavinsky, Vendian lithologic complexes of the world. *Sov.*  
593 *Geol.* **5**, 37–59 (1981).
- 594 106. A. B. Ronov, V. Y. Khain, K. B. Seslavinskiy, Lower and middle riphean lithologic com-  
595 plexes of the world. *International Geology Review* **24**, 509–525 (1982).
- 596 107. D. C. Segessenman, S. Peters, Macrostratigraphy of the Ediacaran System in North Amer-  
597 ica. *Preprint at <https://doi.org/10.31223/X5Z04M>* (2022).
- 598 108. C. B. Keller, B. Schoene, Statistical geochemistry reveals disruption in secular litho-  
599 spheric evolution about 2.5 Gyr ago. *Nature* **485** (2012).
- 600 109. A. J. Fraass, D. C. Kelly, S. E. Peters, Macroevolutionary History of the Planktic  
601 Foraminifera. *Annual Review of Earth and Planetary Sciences* **43**, 139–66 (2015).
- 602 110. A. D. Rooney, F. A. Macdonald, J. V. Strauss, F. Ö. Dudás, C. Hallmann, D. Selby, Re-  
603 Os geochronology and coupled Os-Sr isotope constraints on the Sturtian Snowball Earth.  
604 *Proceedings of the National Academy of Sciences* **111**, 51–56 (2014).
- 605 111. T. M. Gibson, S. Wörndle, P. W. Crockford, T. H. Bui, R. A. Creaser, G. P. Halverson,  
606 Radiogenic isotope chemostratigraphy reveals marine and nonmarine depositional envi-  
607 ronments in the late Mesoproterozoic Borden Basin, Arctic Canada. *GSA Bulletin* **131**,  
608 1965–1978 (2019).
- 609 112. R. Rainbird, A. Rooney, R. Creaser, T. Skulski, Shale and pyrite Re-Os ages from the  
610 Hornby Bay and Amundsen basins provide new chronological markers for Mesoprotero-  
611 zoic stratigraphic successions of northern Canada. *Earth and Planetary Science Letters*  
612 **548**, 116492 (2020).

- 613 113. W. Farrell, J. A. Clark, On postglacial sea level. *Geophysical Journal International* **46**,  
614 647–667 (1976).
- 615 114. R. A. Kendall, J. X. Mitrovica, G. A. Milne, On post-glacial sea level–II. Numerical for-  
616 mulation and comparative results on spherically symmetric models. *Geophysical Journal*  
617 *International* **161**, 679–706 (2005).
- 618 115. G. A. Milne, J. X. Mitrovica, Postglacial sea-level change on a rotating Earth: first results  
619 from a gravitationally self-consistent sea-level equation. *Geophysical Journal Interna-*  
620 *tional* **126**, F13–F20 (1996).
- 621 116. J. X. Mitrovica, J. Wahr, I. Matsuyama, A. Paulson, The rotational stability of an ice-age  
622 earth. *Geophysical Journal International* **161**, 491–506 (2005).
- 623 117. P. Johnston, The effect of spatially non-uniform water loads on prediction of sea-level  
624 change. *Geophysical Journal International* **114**, 615–634 (1993).
- 625 118. G. A. Milne, J. X. Mitrovica, J. L. Davis, Near-field hydro-isostasy: the implementation  
626 of a revised sea-level equation. *Geophysical Journal International* **139**, 464–482 (1999).
- 627 119. K. Lambeck, A. Purcell, P. Johnston, M. Nakada, Y. Yokoyama, Water-load definition in  
628 the glacio-hydro-isostatic sea-level equation. *Quaternary Science Reviews* **22**, 309–318  
629 (2003).
- 630 120. T. Pico, J. X. Mitrovica, K. L. Ferrier, J. Braun, Global ice volume during MIS 3 inferred  
631 from a sea-level analysis of sedimentary core records in the Yellow River Delta. *Quater-*  
632 *nary Science Reviews* **152**, 72–79 (2016).

633 121. A. Dalca, K. Ferrier, J. Mitrovica, J. Perron, G. Milne, J. Creveling, On postglacial sea  
634 level—III. Incorporating sediment redistribution. *Geophysical Journal International* **194**,  
635 45–60 (2013).

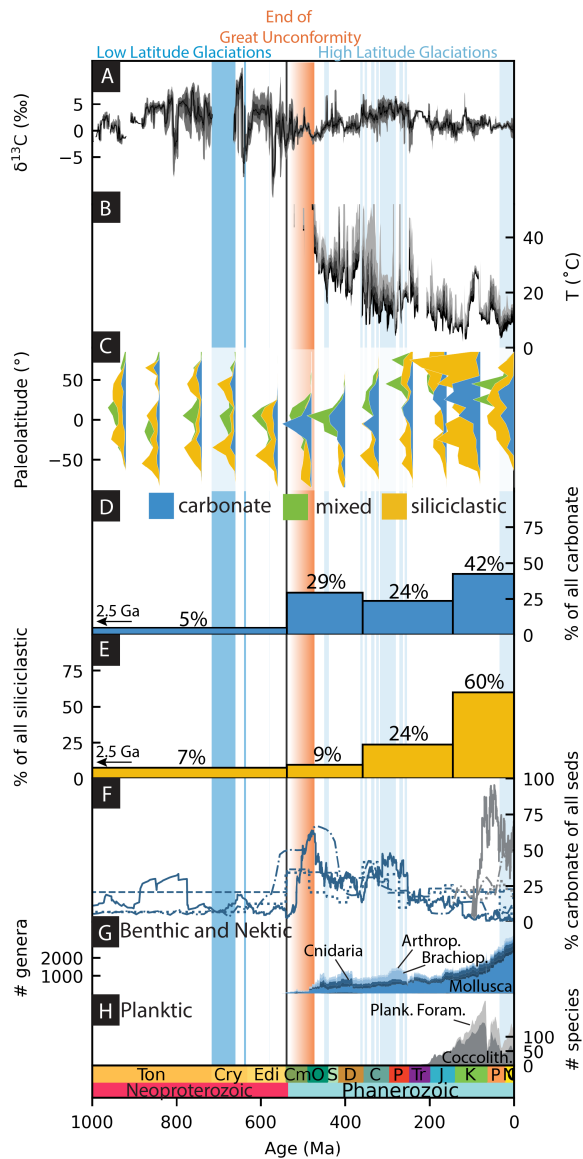
636 **Acknowledgements:** K.D.B. thanks Maggie Osburn, Clint Cowan, and Andy Knoll for pro-  
637 viding comments on early drafts of this work and Jess Adkins for being a sounding board for  
638 ideas. Seth Finnegan assisted with the Paleobiology Database-derived calcifier diversity curves  
639 in Fig. 1G,H. K.D.B. and J.W. thank Shanan Peters for training and encouragement to utilize  
640 the Macrostrat database; **Funding:** K.D.B. acknowledges funding from the Packard Foundation  
641 and NASA Exobiology Grant 80NSSC19K0464. M.D.C. was supported by a National Defense  
642 Science and Engineering Graduate Fellowship; **Author Contributions:** K.D.B. conceptual-  
643 ized the study and wrote the original draft. K.D.B. and J.W. contributed to data investigation,  
644 methodology and data curation. J.W. contributed Macrostrat methodology. N.B. and K.D.B  
645 contributed software, formal analysis, and visualization. T.P. contributed sea level loading esti-  
646 mates in Fig. 2 and Supplement. B.K. contributed EarthChem data and methodology in Fig. 1C  
647 and Fig. 3D. All authors reviewed and edited the manuscript; **Data and materials availability:**  
648 All data are provided in the main text or in the supplementary materials. Data, figures, and  
649 code are available at Open Science Framework (link) for reviewers and will be made publicly  
650 available on manuscript acceptance.

651 **Supplementary Materials** :

652 Materials and Methods

653 Figs. S1 - S10

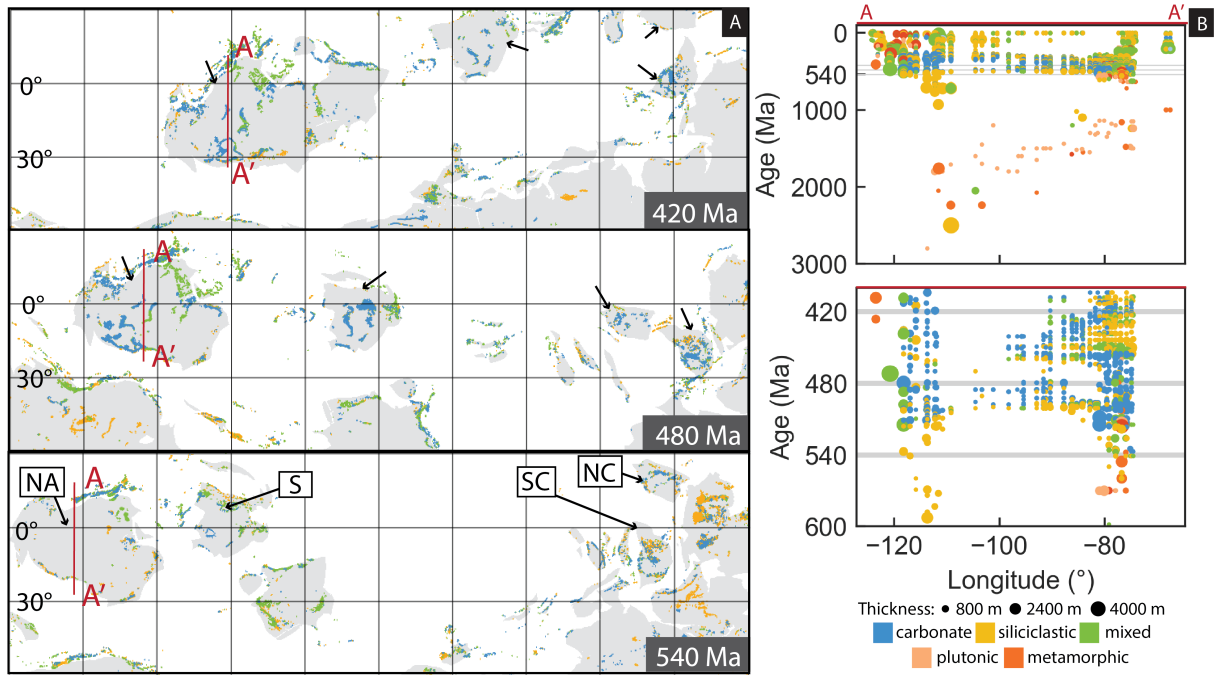
654 References (81 - 120)



655

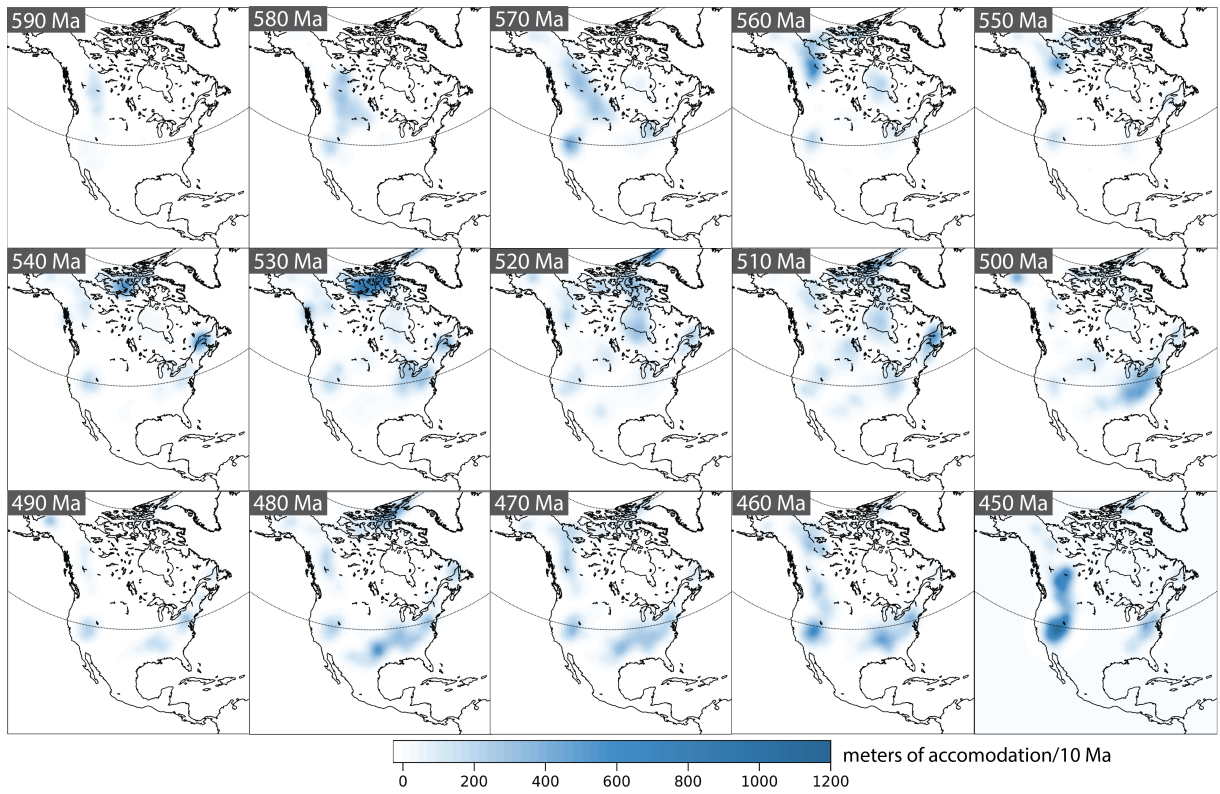
656 **Fig. 1. Carbonate isotopic data, the sedimentary record and calcifier biodiversity (A)**  
 657 Quartiles of  $\delta^{13}\text{C}$  from marine carbonates are plotted every 0.5 Myr with a 4 Myr moving  
 658 window. The second and third quartiles are darkest (3, 83–86). **(B)** Quartiles of temperature  
 659 inferred from fossil  $\delta^{18}\text{O}$  assuming seawater =  $-1.2\text{‰}$  (87) are plotted every 1 Myr with a 4  
 660 Myr moving window (8). The first quartile is the darkest. **(C)** Histograms estimate probability  
 661 density functions of Area ( $\text{m}^2$ ) of three sedimentary rock groups by paleolatitude in 80 Myr

662 bins. The Neoproterozoic probability density function histograms overestimate area because  
663 units have poor temporal resolution. Colors are carbonate (blue), mixed (green), and siliciclas-  
664 tic (yellow) (58). **(D)** The fraction of carbonate area in each bin to total carbonate area. Bins  
665 are 2500–538.8, 538.8–358.9, 358.9–145, 145–0 Ma. **(E)** The fraction of siliciclastic rock area  
666 in each bin to total siliciclastic area. Bins are the same as in d. **(F)** The proportion of car-  
667 bonate to total sediments from our work (continents, dash) (58, 88), previous map-based com-  
668 pilations (continents, blue dot, deep sea, grey dot) (71), named lithologies among EarthChem  
669 sedimentary whole-rock samples (continents, blue dash dot, deep sea, grey dash dot) (89), and  
670 Macrostrat(continents, blue solid, deep sea, grey solid) (18, 29). **(G)** Diversity of benthic and  
671 nektic genera that produce calcium carbonate skeletons (90). **(H)** Diversity of planktic species  
672 of foraminifera and coccolithophores (18, 19). Vertical bars indicate events: two Snowball Earth  
673 glaciations (dark blue), high latitude glaciations (light blue), the end of the Great Unconformity  
674 (orange gradient), the Neoproterozoic–Phanerozoic boundary (bold black line)



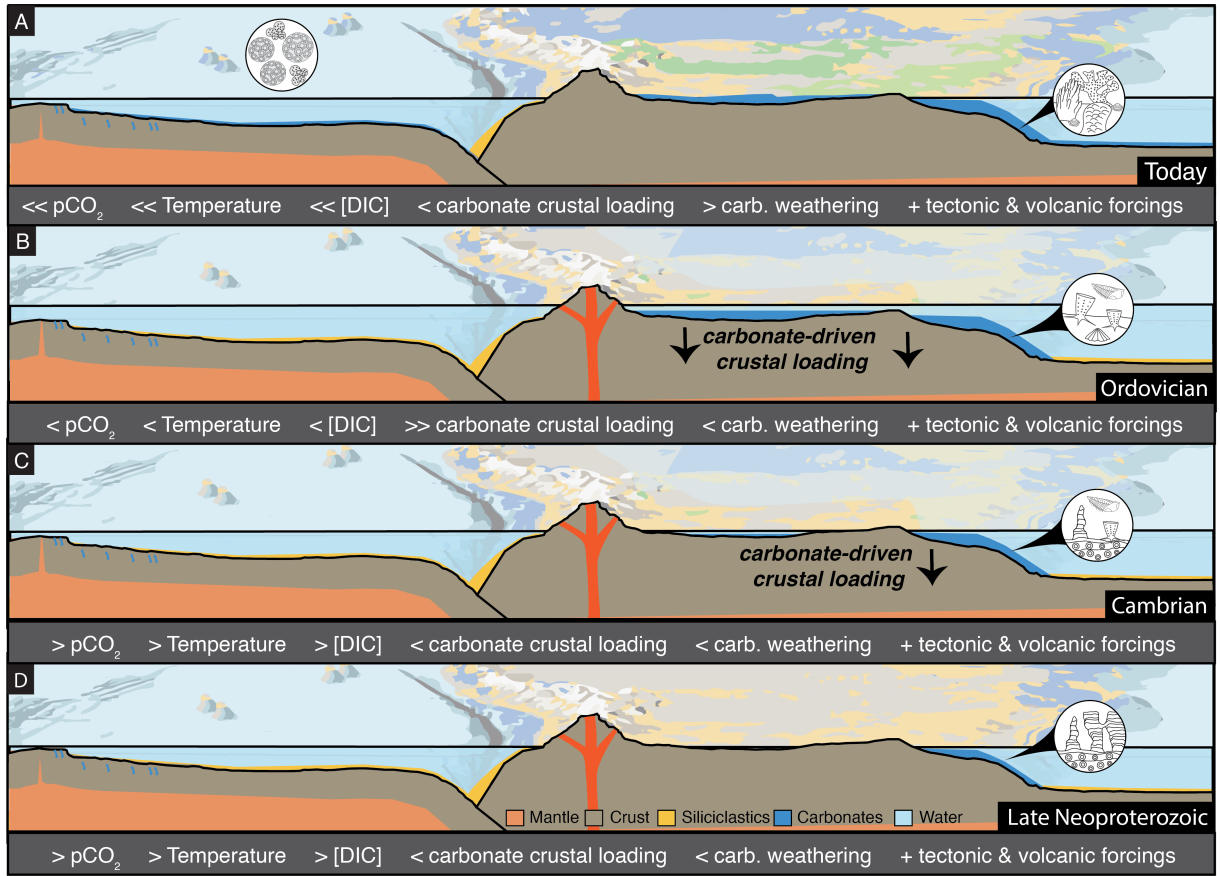
675

676 **Fig. 2. Spatial distribution of sedimentary rocks and sea-level change caused by carbon-**  
 677 **ate loading at the end of the Great Unconformity (A)** Time slices at 540, 480 and 420 Ma  
 678 of surface sedimentary units (58). Equatorial land masses include North America (NA), Siberia  
 679 (S), North China (NC), South China (SC). **(B)** Cross section of the North American continent  
 680 at present-day 40°N (A-A') showing both thickness and age of each unit using data from (29).  
 681 The lower panel zooms into the 600–400 Ma time window. The cross section of A-A' (red) is  
 682 shown in (A). The three time slices from (A) are horizontal grey lines.



683

684 **Fig. 3. Model of carbonate induced accommodation per 10 million year interval.** Unit  
 685 thicknesses are partitioned into carbonate and siliciclastic components based on the unit litho-  
 686 logic description. Carbonate density =  $2710 \text{ kg/m}^3$ . Rock thickness, age, and lithology data  
 687 used to calculate sediment loading are from Macrostrat (29).



688

689 **Fig. 4. Conceptual model of proposed changes in carbonate rock reservoir and Earth**  
 690 **System impacts through time (A)** Today diverse carbonate reef builders and calcifying plank-  
 691 ton effectively sequester CO<sub>2</sub> on continental margins and the deep sea and efficiently reintro-  
 692 duce carbonate to the mantle. Some continent interiors maintain large carbonate reservoirs  
 693 formed during the early Paleozoic. **(B)** Ordovician carbonate platform of biomineral-built reefs  
 694 drives impressive continent-scale progradation of the carbonate platforms and subsidence, ef-  
 695 fectively sequestering CO<sub>2</sub>. **(C)** Cambrian carbonate platform of mixed microbial, abiotic and  
 696 biomineral-built reefs drives continent-scale progradation of the carbonate platforms and subsi-  
 697 dence, effectively sequestering CO<sub>2</sub>. **(D)** Late Neoproterozoic carbonate factory is dominated  
 698 by microbial and abiotic carbonates with small platforms on continental margins.

699 **Supplementary Materials for: Onset of carbonate biomineralization drove global**  
700 **reorganization of sedimentation and subsidence patterns**

701 Authors:

702 Kristin D. Bergmann, Julia Wilcots, Tamora Pico, Nicholas Boekelheide, Noah T. Anderson,

703 Marjorie D. Cantine,

704 Samuel L. Goldberg,

705 Brenhin Keller, Adam B. Jost Athena Eyster

706 **1 Materials and Methods**

707 **Global and Regional Lithologic Estimates** To estimate potential changes in the size and dis-  
708 tribution of the carbonate rock reservoir in the Neoproterozoic and Phanerozoic, we first merged  
709 a recent global lithologic map (88) with continent-scale and regional geologic maps containing  
710 age information from the USGS. The global lithologic map contains about 1.2 million poly-  
711 gons. The map is about 100 times more detailed than previous global lithological maps (88).  
712 This map is paired with USGS maps from Africa (91), Arabia (92), Arctic (93), Asia (94), Eu-  
713 rope (95), Iran (96), North America (97), South America (98), and Russia (99). We assigned a  
714 top and bottom age to each lithologic polygon using the ages of the intersecting polygons from  
715 the USGS maps. We note that most continent-scale and regional geologic maps do not have  
716 good temporal resolution of Proterozoic units (i.e. tags are ‘Proterozoic’ or at best ‘Neopro-  
717 terozoic’) and this represents a source of uncertainty. We recalculated the area of all polygons  
718 for a consistent time-dependent lithologic area estimates. We then used a 1000 Ma–present  
719 day plate reconstruction underpinned by paleomagnetic data (100) in Gplates (101) to calculate  
720 paleolatitude for the centroid of each of our new age-constrained lithology polygons every 20  
721 Myr. We reimported these polygons into ArcGIS to calculate area through time based on age  
722 range and paleolatitude. Data is binned into 80 Myr bins and plotted as histograms (Fig. 1C).

723 To estimate potential changes in continental carbonates since the start of the Neoproterozoic  
724 (1000 Ma), we assessed the area, volume, and proportion of three sedimentary rock groups  
725 through time and space: siliciclastic, carbonate, and mixed sediments (both siliciclastics and  
726 carbonates)(Fig. 1,2). The definitions of our three sedimentary rock groups are defined by the  
727 global lithologic map (88)(Fig. 1C,D, Figs. S1,S3,S4,S5). We summed the area of all carbonate  
728 polygons within four time bins and compared that area to the total area of all carbonate polygons  
729 in our age-delineated global lithologic map dataset (Fig. 1D). We used the same approach with  
730 siliciclastic polygons (Fig. 1E).

731 Despite uncertainties in Neoproterozoic–Ediacaran reconstructions and continental con-  
732 nections ( (50, 102–104)), the paleogeographies especially important for this work (580 Ma–  
733 present) have greater paleomagnetic support and display agreement in paleolatitudes. While the  
734 sedimentary unit area by paleolatitude probability density functions may shift as both global  
735 reconstructions and age ranges of Precambrian geologic units are improved, the important fea-  
736 tures uncovered here, namely the early Phanerozoic increase in low latitude carbonates will  
737 remain unchanged with choice of paleogeographic reconstruction.

738 We also compared estimates of the proportion of carbonate to all sedimentary rocks from  
739 four datasets relevant to the continental rock reservoir (Fig. 1F). The four include: 1) the  
740 proportion of areal extent of carbonates versus total area of sedimentary rocks using our age-  
741 delineation of the global lithologic map dataset from (88)(Fig. 1F, blue dashed line), 2) a  
742 global dataset of area and volume estimated using global lithologic maps created by (32,33,105,  
743 106)(Fig. 1F, blue dotted line), 3) a North America-specific database that includes subsurface as  
744 well as surface geology, estimated maximum and minimum thickness, proportional lithologic  
745 information, and areal extent of each unit (Macrostrat, Project ID 1, (29))(Fig. 1F, blue solid  
746 line). The Ediacaran units have recently been updated (29, 107), and 4) named lithologies of  
747 continental sedimentary whole-rock sample analyses from the large geochemical EarthChem

748 database (89), plotted using weighted bootstrap resampling approach (108)(Fig. 1F, blue dot  
749 dash line). For comparison, we also calculated the proportion of deep-sea carbonates to all  
750 deep-sea sediments since the Jurassic using three available compilations. The three include: 1)  
751 an estimate using drilled ocean sediment cores (33, 71)(Fig. 1F, grey dotted line), 2) a second  
752 estimate using the thickness and estimated areal extent of many more deep sea sediment cores  
753 (Macrostrat Project ID 4) (109)(Fig. 1F, grey solid line), 3) and named lithologies of deep-sea  
754 sedimentary whole-rock samples from the large geochemical EarthChem database (89), plotted  
755 using a weighted bootstrap resampling approach (108)(Fig. 1F, grey dot dash line).

756 We assessed regional lithologic patterns across North America using the higher resolution  
757 surface and subsurface dataset from Macrostrat (Fig. 2B, Fig. S7) (29). To create a 'mixed'  
758 group, we created a new category where the siliciclastic and carbonate proportions of a unit  
759 were each between 45–55%. The Ediacaran units have recently been updated (29, 107). To  
760 better reflect the current state of understanding about Mesoproterozoic and Tonian stratigraphy,  
761 we also adjusted key thickness and depositional age range estimates in the Macrostrat North  
762 America dataset (29). We changed the Little Dal Group thickness from 8000 m to 2500 m in  
763 the Mackenzie Mountains and the Ashburn Formation thickness from 3500 m to 1500 m. We  
764 changed the age range for the Katherine Group to 930–900 Ma and the Little Dal Group to  
765 900–775 Ma across all polygons for consistency (110). We updated the depositional age range  
766 of the Victor Bay and Arctic Bay formations of the Uluksan Group to 1100–1050 Ma (111).  
767 We updated the age range of the Angmaat-Nanisivik Formations (formerly Society Cliffs) of  
768 the Uluksan Group to 1270–1100 Ma (111). In the Shaler Group, we updated the age range of  
769 the Glenelg Formation to 1151–1000 Ma, the Reynolds Point Formation to 1000–850, and the  
770 Wynniatt Formation to 850–795 Ma (112). For our modified Macrostrat Project 1 spreadsheet  
771 see (OSFrepository).

772 **Accommodation Calculation** To calculate the consequence of sediment load on accommo-  
773 dation, we created a grid using all sedimentary rocks listed as deposited between 600–360 Ma  
774 in the North American Macrostrat database (29). Grid resolution is 1° latitude and longitude  
775 and time resolution is 1 Ma. We opted to partition the thickness of a unit to each lithology (i.e.  
776 siliciclastic and carbonate) based on the lithologic description in Macrostrat (29) (Fig. 2, Figs.  
777 S8,S9,S10,S11).

778 To calculate the increase in accommodation ( $\Delta SL$ ) in response to carbonate loading, we  
779 used a gravitationally self-consistent glacial isostatic adjustment model to solve the sea-level  
780 equation (113). We perform calculations based on the theory and pseudo-spectral algorithm  
781 described by Kendall et al. (2005) with a spherical harmonic truncation at degree and order 512  
782 (114). These calculations include the impact of load-induced Earth rotation changes on relative  
783 sea-level (115, 116), evolving shorelines (114, 117–119), and they incorporate a gravitationally  
784 self-consistent treatment of sediment loads (120, 121). We adopt a one-dimensional Maxwell  
785 viscoelastic Earth model VM2, which is characterized by an elastic lithospheric thickness of  
786 120 km, and an average viscosity of  $0.3 \times 10^{21}$  Pa·s and  $3 \times 10^{21}$  Pa·s, for the upper and lower  
787 mantle, respectively.

788 On the multi-million-year timescale relevant for constraining changes in carbonate thick-  
789 ness, we can approximate the solid Earth’s response to loading changes as in isostatic equilib-  
790 rium. Therefore, we adopt the fluid Love numbers associated with the VM2 earth model in our  
791 accommodation calculations. In our modeling, we use a density of 2750 kg/m<sup>3</sup> for carbonate  
792 rocks and 2200 kg/m<sup>3</sup> for siliciclastic rocks. We predict the accommodation change due to  
793 sediment loading every 10 My from 600–360 Ma (Fig. 3, Figs. S10,S11).

794 We use estimates for modern North American lithosphere thickness and mantle rheology  
795 for our model, despite that Earth structure has changed considerably between the early Paleo-  
796 zoic and today, including crustal thickening on the margins from subsequent mountain-building

797 events. Such an assumption is required given the challenges associated with reconstructing  
798 mantle dynamics in deep time (59). Although our predictions will vary with different selected  
799 Earth rheology parameters, our results offer a robust first-order assessment of sediment loading  
800 across 600-360 Ma.

## 801 **2 Supplementary information**

802 **Fig. S1** To fully explore the global patterns in each continental sedimentary rock reservoir,  
803 we considered the total area of each reservoir through time (Fig. S1A), the time normalized  
804 total area (Fig. S1B), the proportion of each reservoir to the total sedimentary reservoir through  
805 time (Fig. S1C) using our age-delineation of the global lithologic map dataset from (88). To  
806 explore the contribution of different time periods to each of the continental carbonate and sili-  
807 ciclastic rock reservoirs, we binned the carbonate area relative to the total continental carbonate  
808 area and the siliciclastic area relative to the total siliciclastic area (Fig. S1D). Lighter blue  
809 and yellow bin [358.9, 358.9–145, 145–0 Ma] and darker blue and yellow bins are [1000–  
810 538.8, 538.8–486.9, 486.9–443.1, 443.1–419, 419–359.3, 359.3–323.4, 323.4–307, 307–298.9,  
811 298.9–251.9, 251.9–201.4, 201.4–143.1, 143.1–66, 66–56, 56–33.9, 33.9–23.04, 23.04–5.33,  
812 5.33–2.58, 2.58–0.0117, 0.0117–0 Ma] respectively. To explore the importance of the mixed  
813 group we added 20% of the mixed area to the carbonate bins (lightest blue) and 80% of the  
814 mixed area to the siliciclastic bins (lightest yellow). This does not significantly alter the rel-  
815 ative contribution of any bin. The proportion of carbonates and siliciclastics to total area of  
816 each reservoir in the four longer time bins do not follow the same pattern. Proterozoic rocks  
817 are a minor contribution to the total carbonate reservoir (5%) especially when compared to  
818 the large early Phanerozoic carbonate contribution (29%, Fig. 1D). In contrast, the siliciclas-  
819 tics within these time intervals represent a minor proportion of all siliciclastic rocks (Protero-  
820 zoic: 7% and Early Phanerozoic: 9%), Fig. 1E). Indeed, younger siliciclastic rocks are an

821 increasingly large portion of their total reservoir whereas the fraction of carbonate is more sta-  
822 ble across the Phanerozoic. Mixed depositional systems show a modest increase in area across  
823 the Neoproterozoic–Phanerozoic boundary. Taking their contribution into account in each time  
824 bin, the time-varying proportions of carbonates and siliciclastics barely change (Fig. 1C), Fig.  
825 S1). Most continent-scale geologic maps do not have good temporal resolution of Proterozoic  
826 units (i.e., tags are "Proterozoic" or "Neoproterozoic") and this represents a source of uncer-  
827 tainty. We chose to bin the entire Proterozoic in Fig. 1C,D for this reason, which makes the  
828 differences between carbonate and siliciclastic rock in the Proterozoic and Early Phanerozoic  
829 bins even more surprising.

830 **Fig. S2** We calculate rough estimates of CO<sub>2</sub> sequestration in GtC/yr into the continental and  
831 deep sea carbonate rock reservoirs through time based on the current, preserved sedimentary  
832 rock record (Fig. S2A). To calculate volume from our age-delineated, global lithologic map  
833 dataset from (88), we assumed a constant carbonate thickness of 178 m over the entire time  
834 interval and all regions (Fig. S2, blue dashed lines). This represents the average maximum  
835 thickness of carbonate units in North America from Macrostrat (29). We compare this estimate  
836 of the flux of GtC/yr to one using the Macrostrat North America and deep sea projects (projects  
837 = 1 and 4) (29, 109)(Fig. S2, blue and grey solid lines). For the deep sea database we only  
838 calculate volume using the thickness data in combination with the area of the Atlantic Ocean  
839 as that is where most of the cores in Project ID 4 are from (109). Without a better resolved  
840 global ocean time series, this is only a rough estimate of the GtC/yr sequestered in the deep  
841 sea carbonate reservoir. We also include an estimate of GtC/yr sequestered into the two car-  
842 bonate rock reservoirs from global dataset of area and volume estimated using global lithologic  
843 maps created by (32, 105, 106)(Fig. S2, blue dotted line)and the deep sea using drilled ocean  
844 sediment cores (33, 71)(Fig. S2, grey dotted line) (Fig. S2). We use the burial flux from the

845 existing map based area (88) and the Macrostrat-based deep sea burial flux estimate (29, 109)  
846 to estimate residence time of inorganic carbon in the ocean using the modern size of the DIC  
847 reservoir over the entire time interval (38973 GtC) and with a larger reservoir in the Precam-  
848 brian and early Paleozoic that was ultimately sequestered in early Paleozoic carbonates (101000  
849 GtC). Residence time increases to 1-2.5 million years in the Precambrian if one assumes shal-  
850 low nearshore environments are the dominant carbonate sequestering environment before the  
851 evolution of planktonic calcifying organisms (Fig. S2B).

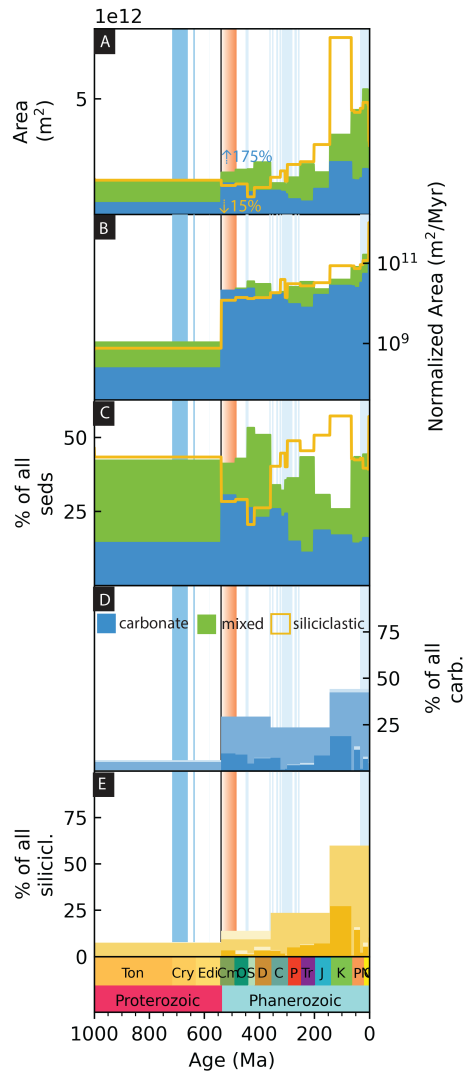
852 **Figs. S3,S4** We explore changes in area and proportion of each lithology at the regional-scale  
853 and note the locations with significant increases in sedimentary rocks across the Proterozoic–  
854 Phanerozoic transition are dominated by carbonate (Figs. S3,S4).

855 **Figs. S5,S6, Movie S1** To explore the data at the most granular map scale through time we  
856 use ArcGIS to replot the lithologic polygons from our age-delineation of the global lithologic  
857 map dataset from (88) with centroid paleolatitude constraints from the plate reconstruction  
858 by (100) in Gplates (101) every 10 Myr. For comparison, we also include different geologic  
859 maps of North America, Siberia, and China from Macrostrat denoting Ediacaran rocks (pink)  
860 and Cambrian–Ordovician rocks (greens)(Fig. S6) (29). If anything this comparison suggests  
861 the global lithologic map from (88) might underestimate the area of Cambrian–Ordovician sed-  
862 imentary rocks in North America, Siberia and China.

863 **Fig. S7** To visualize the dynamics of carbonate sedimentation across North America in more  
864 detail, we create cross sections of the North American continent at present-day 40°N (Fig.  
865 2c), 35°N, 65°N, 90°W, 120°W (Fig. S7) showing both thickness and age of each unit (i.e., a  
866 Wheeler Diagram) using data from (29). We partitioned the units in siliciclastic and carbonate  
867 thicknesses using Macrostrat lithologic descriptions (Figs. 2C, S7). To create a 'mixed' group,

868 we created a new category where the siliciclastic and carbonate proportions of a unit were  
869 between 45–55%.

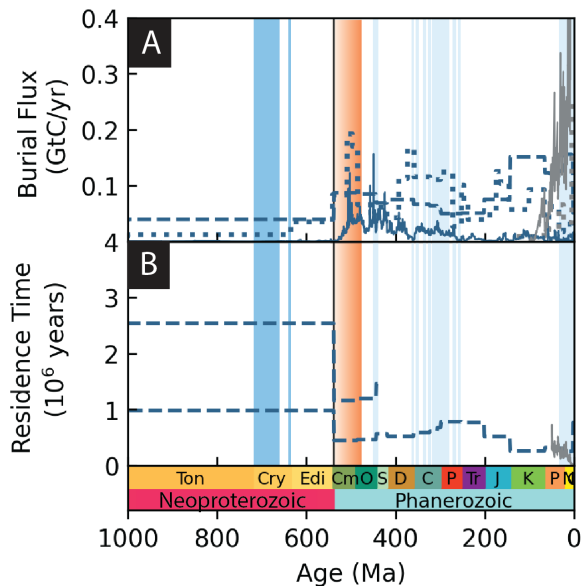
870 **Figs. S8, S9, S10** To understand the predicted sea-level contribution from sediment loading  
871 by siliciclastic and carbonate lithologies, we first binned the loads into three 60 million year  
872 intervals (Fig. S8). To better compare across lithologies, Fig. S8 uses a color bar from 0–  
873 2000 m/60 Myr where the most saturated color represents the maximum accommodation from  
874 carbonate loading. We explored the more granular contribution to accommodation from each  
875 lithology in 10 Myr intervals (Figs. S9,S10).



876

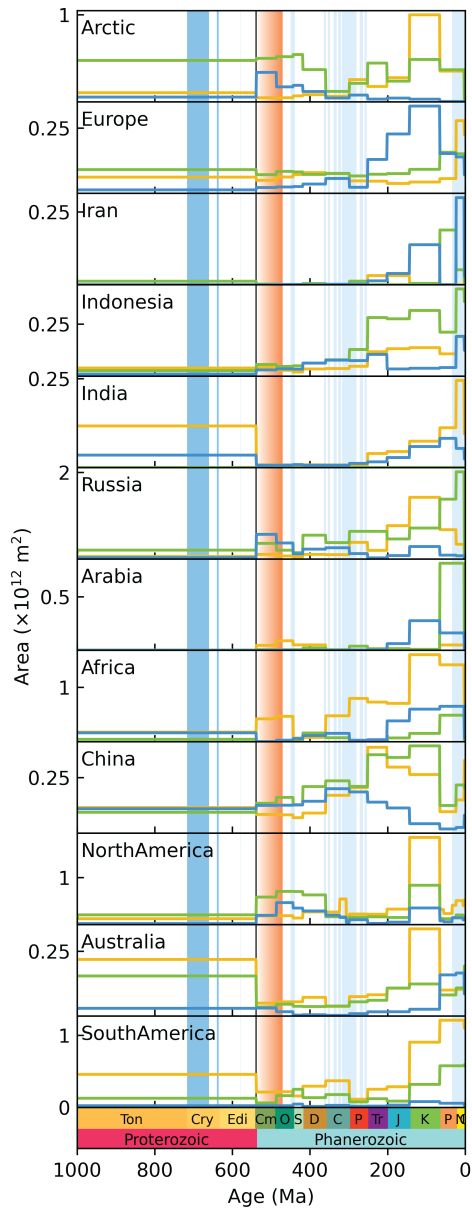
877 **Fig. S1. Total area and proportion of sediments through time.** (A) Area of exposed sedimen-  
 878 tary rocks calculated by combining a global lithologic map (88) and continent-scale geologic  
 879 maps (91–99). The Neoproterozoic areas are overestimates because units have poor tempo-  
 880 ral resolution. (B) Area of exposed sedimentary rocks divided by the duration of the time bin  
 881 ( $\text{m}^2/\text{Myr}$ ). (C) The proportion of each rock type compared to all sedimentary rocks within a  
 882 given time bin. (D) Percent of carbonate rocks to all carbonate rocks within two sets of time  
 883 bins (blue) and assuming 20% of mixed sedimentary rocks are also carbonate (lighter blue).

884 (E) Percent of siliciclastic rocks to all siliciclastic rocks within two sets of time bins (yellow)  
885 and assuming 80% of mixed sedimentary rocks are also siliciclastic (light yellow) (58). Vertical  
886 bars indicate events: two Snowball Earth glaciations (dark blue), high latitude glaciations (light  
887 blue), the end of the Great Unconformity (orange gradient), the Neoproterozoic–Phanerozoic  
888 boundary (bold black line).



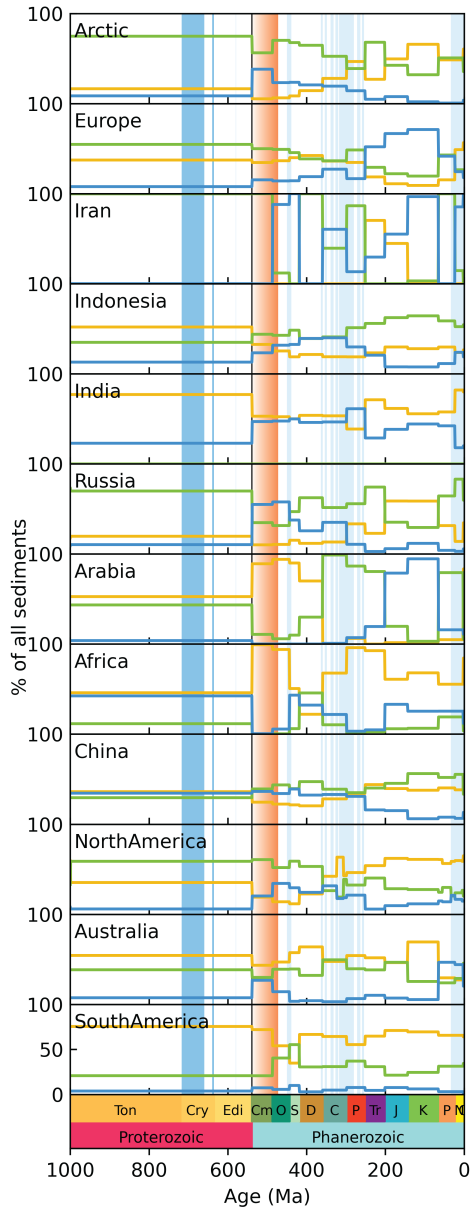
889

890 **Fig. 5. Inorganic carbon burial flux and residence time** (A) Estimates of marine inorganic  
 891 carbon burial flux in GtC/yr (See Methods) using the global lithologic map dataset (continents,  
 892 dash) (88), previous map-based compilations (continents, blue dot, deep sea, grey dot) (71),  
 893 and Macrostrat(continents, blue solid, deep sea, grey solid) (18, 29). All estimates support an  
 894 increase in carbon sequestration in the early Phanerozoic. (B) Estimates of residence time in  
 895 millions of years using the global lithologic map-based burial flux estimate (continents, dash)  
 896 and two DIC pool sizes, 38973 GtC (modern) and 101000 GtC (Precambrian-Ordovician), and  
 897 the Macrostrat-based deep sea burial flux estimate, grey solid) (18, 29) (58). Vertical bars indi-  
 898 cate events: two Snowball Earth glaciations (dark blue), high latitude glaciations (light blue),  
 899 the end of the Great Unconformity (orange gradient), the Neoproterozoic–Phanerozoic bound-  
 900 ary (bold black line).



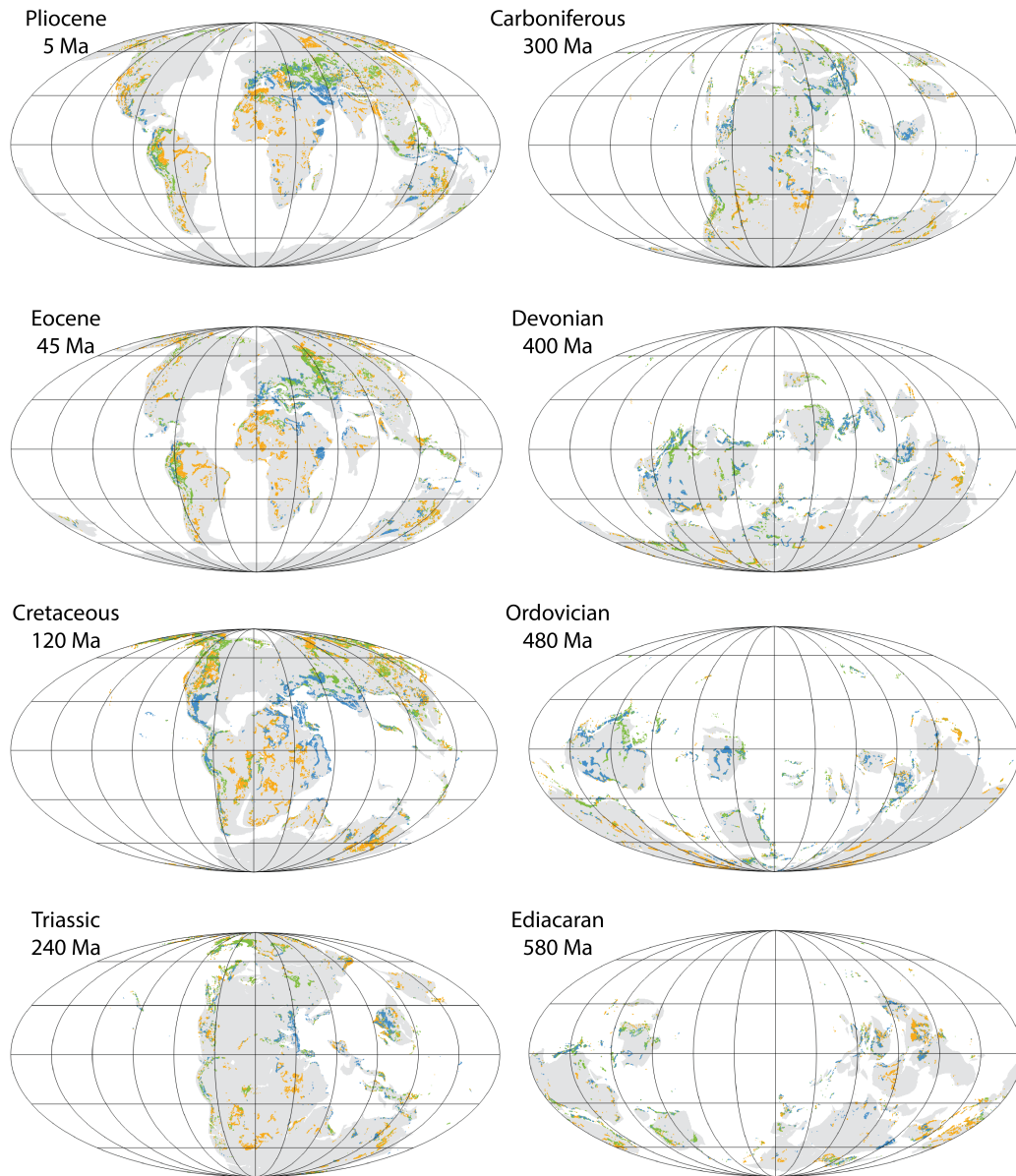
901

902 **Fig. S3. Total area of sedimentary rock types by region** Carbonate (blue), siliciclastic (yel-  
 903 low), mixed carbonate-siliciclastic (green). Vertical light blue boxes indicate periods of glacia-  
 904 tion. The bold vertical line indicates the Neoproterozoic–Phanerozoic boundary.



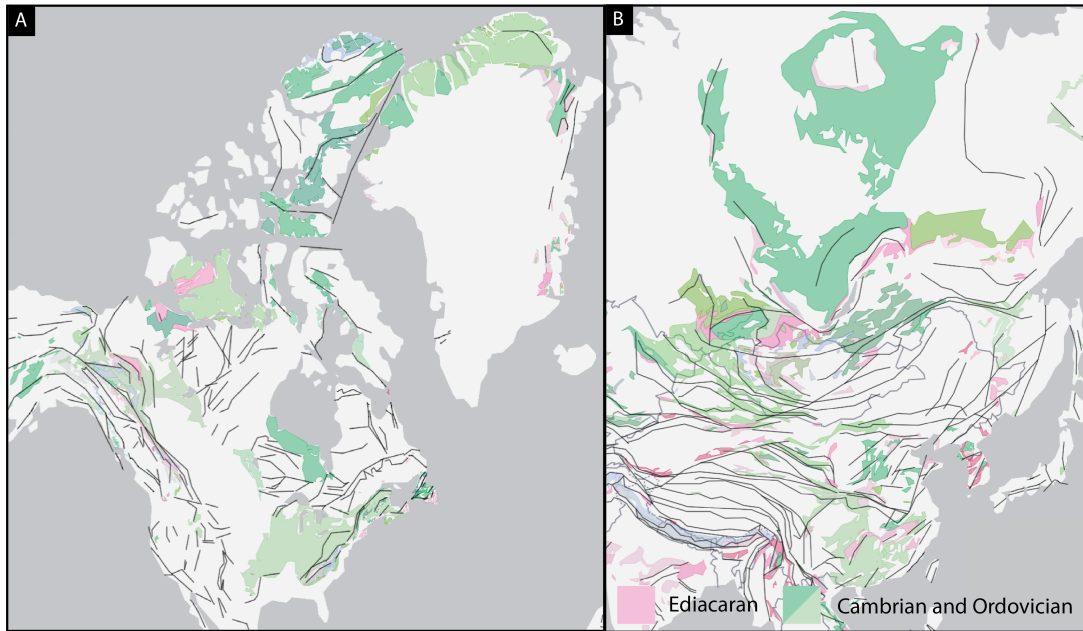
905

906 **Fig. S4. The proportion of sedimentary rock types by time by region.** Carbonate (blue),  
 907 siliciclastic (yellow), mixed carbonate-siliciclastic (green). Vertical light blue boxes indicate  
 908 periods of glaciation. The bold vertical line indicates the Neoproterozoic–Phanerozoic bound-  
 909 ary.



910

911 **Fig. S5. Series of global lithologic maps through time.** Area of exposed sedimentary rocks  
 912 calculated by combining a global lithologic map (88) and continent-scale geologic maps (91–  
 913 99). Carbonate: blue, siliciclastic: yellow, mixed carbonate-siliciclastic: green.

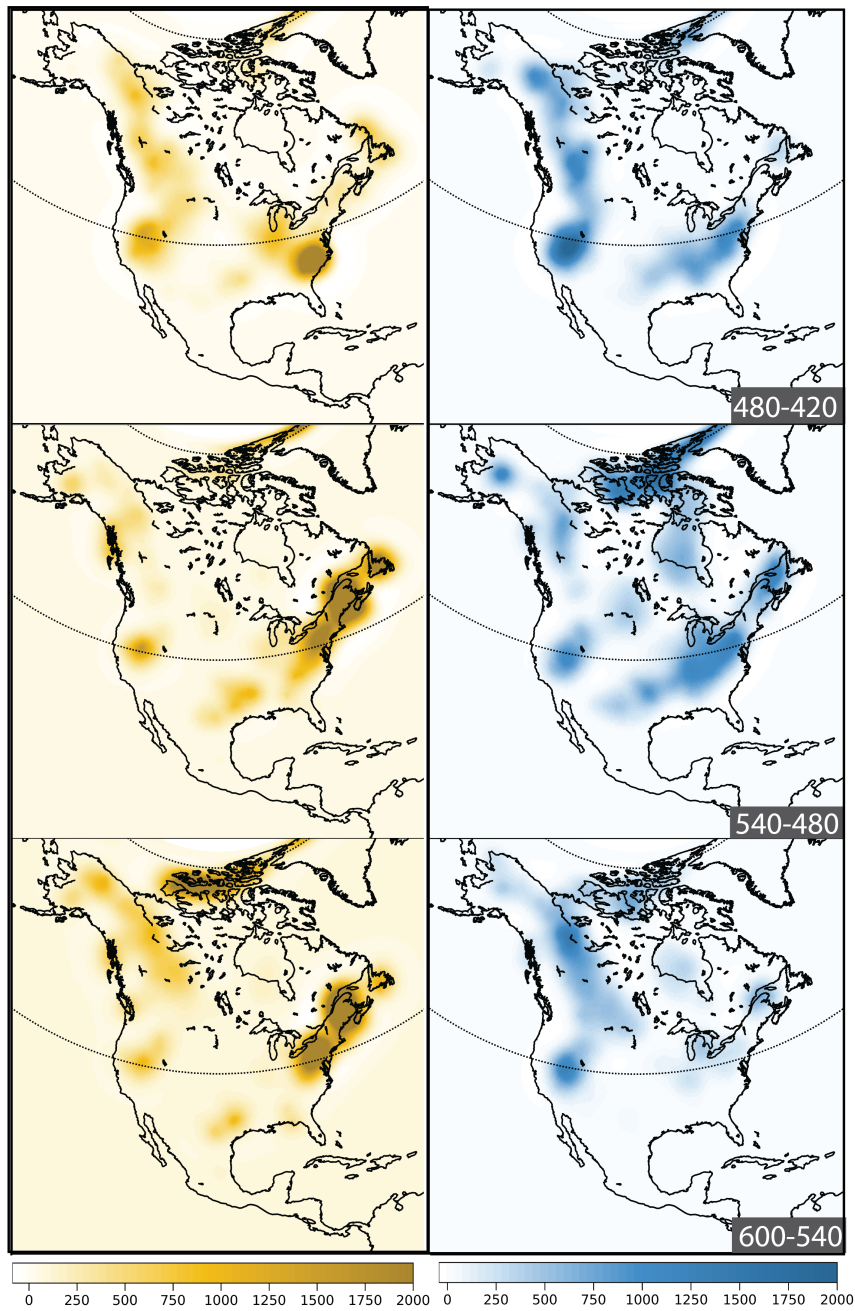


914

915 **Fig. S6. Map of Ediacaran and Cambrian–Ordovician aged rocks from Macrostrat. (A)**  
 916 **Map of Ediacaran and Cambrian–Ordovician aged rocks in North America. (B) Map of Edi-**  
 917 **acaran and Cambrian–Ordovician aged rocks in Siberia and Asia. Filtered map from Macrostrat**  
 918 **of Ediacaran (pink) rocks and Cambrian–Ordovician rocks (greens) (29). Most are sedimentary**  
 919 **rocks but not all.**



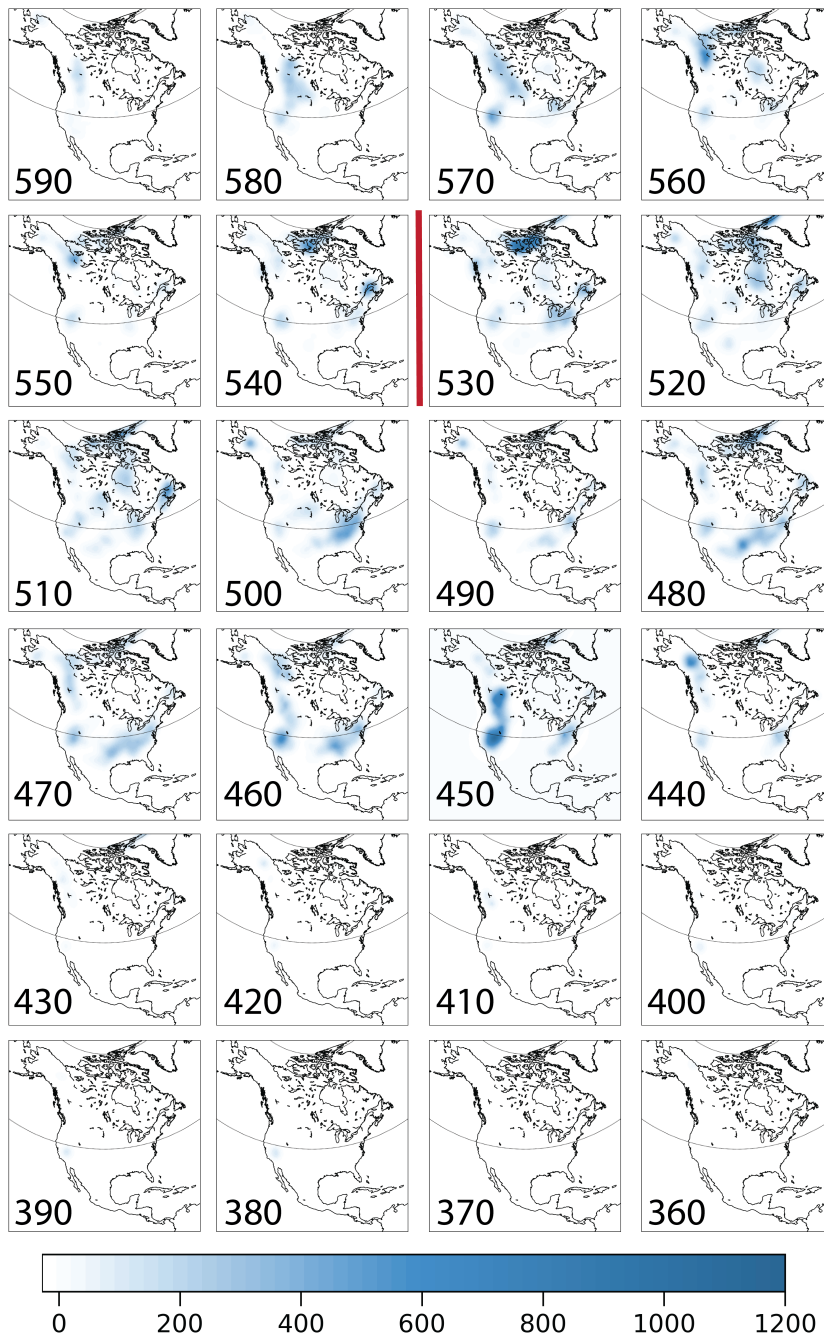
924 loading are from Macrostrat (29). Carbonate: blue, siliciclastic: yellow, mixed carbonate-  
925 siliciclastic: green, igneous and metamorphic: pink and red.



926

927 **Fig. S8. Model of siliciclastic and carbonate induced accommodation per 60 million year**  
 928 **interval.** Bins are 600–540, 540–480, 480–420 Ma. Color bars for siliciclastic-driven (yellow)  
 929 and carbonate-driven (blue) accommodation are saturated for carbonate (2000 m/60 Myr), while  
 930 siliciclastic rocks can create up to 6000 m/60 Myr of accommodation at their maximum (i.e. the

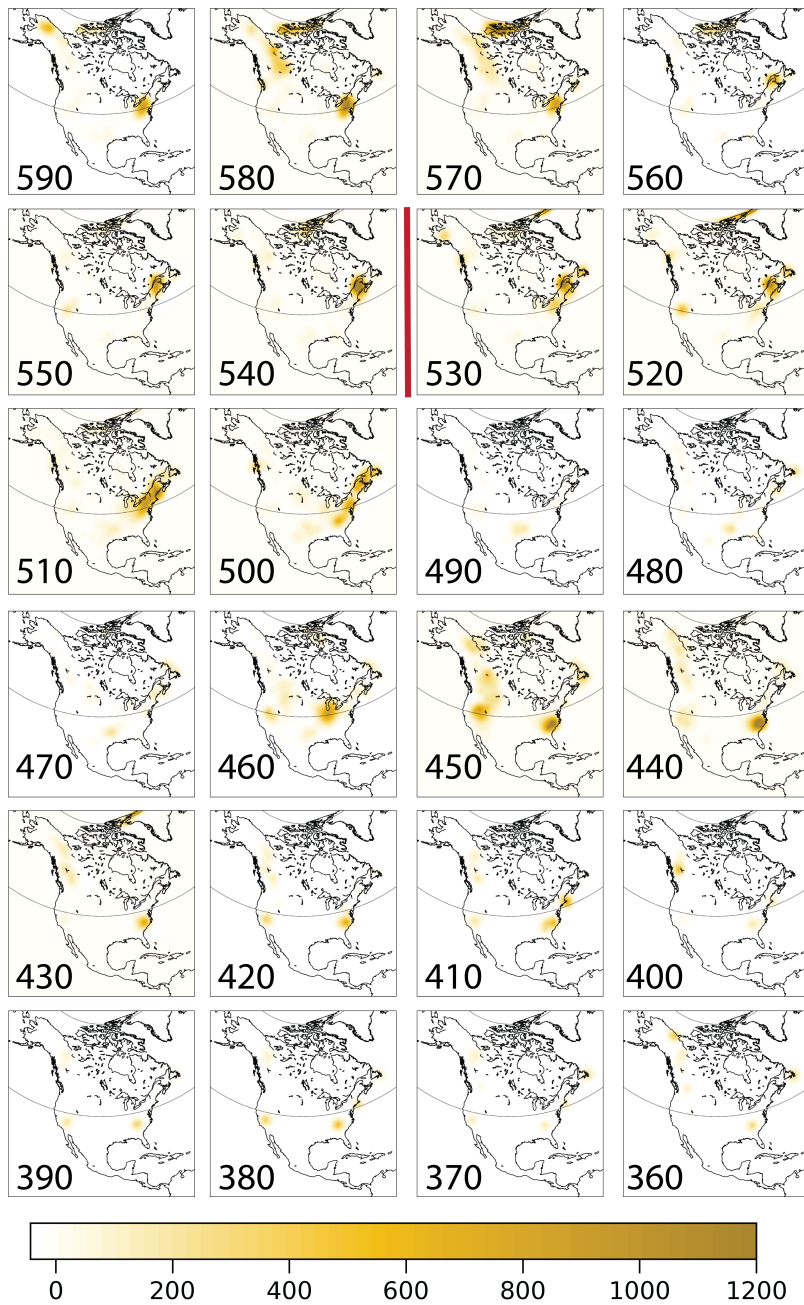
931 Taconic Orogeny). Unit thicknesses are partitioned into carbonate and siliciclastic thicknesses  
932 based on the unit lithologic description. Carbonate density =  $2710 \text{ kg/m}^3$ , and siliciclastic  
933 density =  $2200 \text{ kg/m}^3$ . Rock thickness, age, and lithology data used to calculate sediment  
934 loading are from Macrostrat (29).



935

936 **Fig. S9. Model of carbonate induced accommodation per 10 million year interval.** Unit  
 937 thicknesses are partitioned into carbonate and siliciclastic components based on the unit litho-  
 938 logic description. Carbonate density =  $2710 \text{ kg/m}^3$ . Red line identifies the interval containing

939 the Neoproterozoic-Phanerozoic boundary. Rock thickness, age, and lithology data used to  
940 calculate sediment loading are from Macrostrat (29).



941

942 **Fig. S10. Model of siliciclastic induced accommodation per 10 million year interval.** Unit  
 943 thicknesses are partitioned into carbonate and siliciclastic components based on the unit litho-  
 944 logic description. Siliciclastic density =  $2200 \text{ kg/m}^3$ . Red line identifies the interval containing  
 945 the Neoproterozoic–Phanerozoic boundary. Rock thickness, age, and lithology data used to

946 calculate sediment loading are from Macrostrat (29).